



**UNIVERSITÀ
DEGLI STUDI
DI PADOVA**

Department of Industrial Engineering DII

MASTER OF SCIENCE IN AEROSPACE ENGINEERING

**LARGE EDDY SIMULATION WITH WALL-STRESS
MODEL: AN APPLICATION TO TURBULENT
COMPRESSIBLE CHANNEL FLOW**

Thesis advisor:

Ing. FRANCESCO DE VANNA, PhD

Thesis co-advisor:

Prof. FRANCESCO PICANO

Candidate:

MICHELE COGO

Matriculation number:

1190624

Academic Year 2019/2020

To Linda, for your support during these years

SOMMARIO

In questo lavoro di tesi si vuole descrivere la teoria e l'implementazione di un modello di parete basato su un sistema di equazioni differenziali ordinarie applicato alla tecnica di Large Eddy Simulation (LES). Questa tecnica è stata usata per simulare un flusso turbolento compressibile in un canale. L'applicazione di un modello che simuli la fisica di un flusso vicino a parete fa parte della famiglia di approcci chiamati Wall Modelled Large Eddy Simulation (WMLES) che mirano ad alleggerire il peso computazionale di una simulazione LES evitandone il compito di dover risolvere le strutture turbolente vicino a parete. La tecnica LES è una tecnica molto versatile capace di catturare la natura multiscala e non stazionaria di un flusso turbolento ma è spesso inutilizzabile nei solutori commerciali a causa del suo costo computazionale, soprattutto all'aumentare del numero di Reynolds.

La tecnica che viene invece utilizzata dalla quasi totalità del mondo dell'industria è la Reynolds Averaged Navier-Stokes (RANS) che fornisce le caratteristiche del flusso mediate ma è molto meno restrittiva in termini di tempo macchina quindi è l'unica che può fornire attualmente risultati in tempi ragionevoli per rispondere alle richieste del mercato. L'intento di questo lavoro di tesi è quello di provare la bontà dell'approccio WMLES in un tipico flusso di parete (il canale) per provare come questa tecnica possa avere gli stessi vantaggi della comune LES ad un costo computazionale comparabile a quello di una RANS. I primi capitoli della tesi sono rivolti a dare le basi dei flussi turbolenti ed in particolare del flusso in un canale. In seguito vengono analizzati le principali tecniche attualmente disponibili per la simulazione di flussi con particolare attenzione alla famiglia degli approcci WMLES. Vengono in seguito esposte le equazioni che regolano il modello di parete scelto e la loro implementazione. Infine sono presentati i risultati per flussi incomprimibili e comprimibili, traendone le conclusioni che discutono l'efficacia del modello utilizzato.

Contents

1	Introduction	1
2	Turbulent flows basics	3
2.1	Kolmogorov's theory	3
3	Channel flow	4
3.1	RANS equations of channel flow	5
3.2	Mean velocity profiles	8
3.3	Reynolds stresses	10
3.4	Turbulent kinetic energy budget	10
4	Computational fluid dynamics	11
4.1	Compressible Large eddy simulation	12
4.2	The wall-adaptive Large-Eddy viscosity model	14
5	WMLES overview	15
5.1	Wall stress models	15
5.1.1	Algebraic implementation	16
5.1.2	PDE implementation	16
5.1.3	ODE implementation	17
5.2	Further considerations on the Equilibrium Wall-Modeled Energy Equation	19
6	Discretization of the wall-stress model equations	20
6.1	Discretization of the momentum equation	20
6.2	Discretization of the total energy equation	20
6.3	Numerical aspects of wall stress model	22
6.4	Coupling LES to wall stress model	22
7	Simulation at Mach = 0.1	25
7.1	Pressure-driven turbulent channel	26
7.2	$Re_\tau = 395$	27
7.3	$Re_\tau = 590$	28
7.4	$Re_\tau = 1000$	29
7.5	$Re_\tau = 2000$	30
7.6	Comments to the results	31
8	Simulation at Mach = 1.5	32
8.1	$Re = 500$	32
8.2	$Re = 1010$	33
8.3	Comments to the results	34
9	Conclusions	36

A Appendix - Navier-Stokes Equations **37**

- A.1 Divergence Theorem 37
- A.2 Reynolds transport theorem 37
- A.3 Conservation of mass 37
- A.4 Conservation of Momentum 38
- A.5 Conservation of energy 38

1 Introduction

In our everyday life the majority of both naturally and industrially occurring flows are turbulent, for example flows in rivers, the flows in pipes and combustion engines, the flow of the wind around buildings, cars, ships, etc. The ubiquity of turbulence has led to extensive studies by the scientific community, revealing its very complex nature. To give a sense of the challenging task that the study of turbulence has posed to scientists we can cite the words of the prominent fluid dynamicist Horace Lamb, that reportedly said

‘I am an old man now, and when I die and go to heaven there are two matters on which I hope for enlightenment. One is quantum electrodynamics, and the other is the turbulent motion of fluids. And about the former I am rather optimistic’.

Mathematically the motion of a fluid is governed by the Navier Stokes equations (A.5) but unfortunately it’s rarely possible to solve these non-linear partial differential equation analytically. However, the advent of computers has led to the development of several numerical methods that through a process called discretization can solve these equations using a finite number of values. Analyzing a typical turbulent flow physicists have revealed that the size of coherent three-dimensional vortical structures, so-called eddies, varies from the length of the geometry of the flow to several orders of magnitude less. This consideration implies that the simulation of a turbulent flow requires a computational grid that is dense enough to resolve the smallest scales (which is true in the direct numerical simulation approach, (DNS), however this requirement is often impossible to satisfy because even the most advanced computers can fail to provide a solution in a reasonable amount of time. This issue has led to the development of turbulence modelling, which refers to deriving different sets of equations, based on the original Navier-Stokes equations, where the effect of the smallest eddies on the largest one (that are directly computed) is represented by new simpler terms.

The most commonly used scale-resolving approach in the academic world is Large eddy simulation (LES), in which the large eddies are resolved, whereas the smaller ones are modelled. One of the most important choices in LES approach is the size of the eddies where to start applying the model, and this decision has to be made in order that the model can represent effectively the sub-grid scales in any circumstance, trying to be as coarse as possible to save computational time. One major challenge in this decision is posed by solid boundaries, where the flow loses part of its momentum due to friction. Given the fact that in these regions the fluid rapidly transitions from zero at the wall to the velocity of the free stream, the scales of motion are dynamically important (which means that they must be resolved by the LES grid) but are also order of magnitude smaller than the outside of the boundary layer. As a result the majority of the computational effort is dedicated to the near-wall region.

According to Chapman (1979) [3] and Choi and Moin (2012) [4], who estimated and contrasted the number of computational grid points necessary to resolve the near-wall eddies for direct numerical simulation (DNS), wall-resolved LES (WRLES) and wall-modeled LES (WMLES), the number of computational grid points scale with the Reynolds number (based on the streamwise length) as $N_{DNS} \sim Re_L^{37/14}$, $N_{wr} \sim Re_L^{13/7}$, and $N_{wm} \sim Re_L$ for DNS, WRLES, and WMLES respectively. Although WRLES has a more favorable

scaling than DNS, the near-quadratic Reynolds number dependence of the number of grid points renders such an approach infeasible for realistic configurations. Thus, a strategy where only the outer-layer eddies are resolved and the near-wall eddies scaling in size with viscous units are modeled is required [2].

This thesis deals with this problem in a turbulent channel flow trying to implement a wall model which objective is to allow a coarse (not wall-resolved) LES grid but enforcing the correct local wall shear stress (the friction force between the fluid and the wall per unit contact area) and heat conduction to the wall. In Chapter 2, the basics of turbulent flows are reviewed. Chapter 3 introduces some analytical results of turbulent channel flow. Following that, Chapter 4 gives an overview of the main approaches used in the present time for computational fluid dynamics, focusing on Large eddy simulation (that will be used for the simulations). In Chapter 5 are presented the various approaches for wall modelled large eddy simulation and a detailed description of the theory of an ordinary differential equations wall stress model. Chapter 6 deals with the numerical implementation of the ODE-based wall stress model and its coupling to the LES technique. In Chapters 7 and 8 are presented the results obtained at $Mach = 0.1$ and $Mach = 1.5$ considering various Reynolds numbers. Finally, concluding remarks are given in Chapter 9.

2 Turbulent flows basics

Defining turbulence is a challenging task, but according to Lesieur [13] it has three main features:

- Turbulent flow must be chaotic, so small perturbances to initial conditions lead to completely uncorrelated fields
- Turbulence has the ability to transport and mix fluid much more effectively than a comparable laminar flow
- The scales at which this mixing occurs should include a wide range of spatial wave lengths

It has been shown that turbulence creates and sustains itself in rotational flow, in which the velocity gradients are able to overcome the damping of molecular viscosity to provide small initial perturbations that are transformed into larger scale motions [7]. The turbulent motions range in size from the width of the flow geometry to much smaller scales, which become progressively smaller as the Reynolds number increases. An important concept in turbulence first introduced by Richardson [21] is the *energy cascade*, where the idea is that kinetic energy enters the turbulence at the largest scales of motion and is then transferred by inviscid processes to smaller scales until it is dissipated by viscous action. The size of the smallest eddies that are responsible for dissipating the energy has been investigated by Kolmogorov [11], who developed one of the most important theories of turbulence research.

2.1 Kolmogorov's theory

If we take as l_0 the length of the largest eddies and l the length of a general eddy there are three main hypothesis that lay the foundations of Kolmogorov's theory:

- The small-scale turbulent motions ($l \ll l_0$) are statistically universal and isotropic
- The statistics of the small-scale turbulent motions ($l \ll l_0$) are uniquely determined by ν (kinematic viscosity) and ϵ (energy dissipation)
- If we define η as the scale where dissipation occurs, the statistics of the small-scale turbulent motions ($\eta \ll l \ll l_0$) are uniquely determined by ϵ

From this hypothesis it's possible to divide the scales of turbulent motion in three main sections (characterized by the wavenumber k):

- The energy-containing scales, k_i , where turbulent energy is introduced to the system
- The inertial sub-range, that is dominated by inertial forces rather than viscosity. These scales contain and dissipate very little turbulent energy, but transfer the energy from the largest scales to the smallest
- The dissipative range, k_d , in which the scales are smaller than the Kolmogorov scale, $\eta = (\nu^3/\epsilon)^{1/4}$. In this range the viscous effects strongly damp the turbulent motion, dissipating the turbulent kinetic energy into heat

Using dimensional analysis Kolmogorov was able to quantify the turbulent energy spectrum in the inertial sub-range, which is expressed graphically as a line of constant slope

$$E(k) = C_k \epsilon^{2/3} k^{-5/3} \quad (2.1)$$

where C_k is a universal constant of the order of 1.5. Note that equation (2.1) can only exist if the Reynolds number is high enough that the energy containing and dissipation scales are well separated.

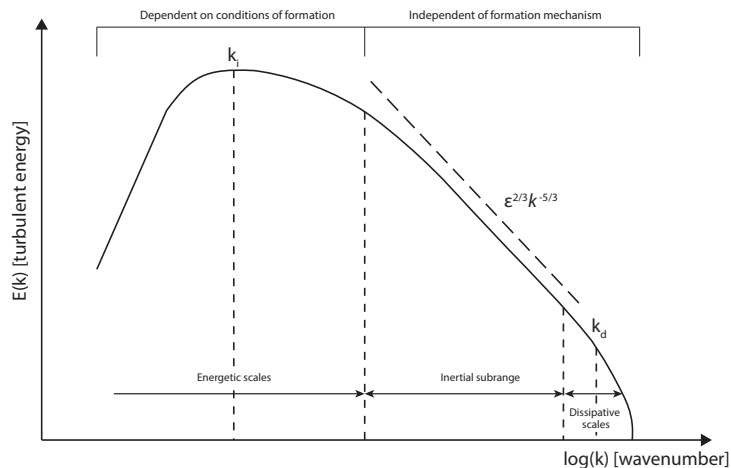


Figure 1: Turbulent energy spectrum (adapted from Hinze [10])

The conversion of bulk fluid kinetic energy into turbulent energy can be divided into two broad categories: free-shear flows such as mixing layers, jets and wakes and wall-bounded flows such as boundary layers, pipes and channels. While in free shear flows the growth of instabilities is essentially an inviscid process and the most energetic structures are large (hence the small scales tend to obey Kolmogorov's law), in wall-bounded flows the limiting influence of a solid boundary on the scales of motion means that primary instabilities develop through a viscous process, that may or may not induce inviscid secondary instabilities. The presence of the wall also poses a physical limit to the growth of the instabilities, so that the resulting vortices are restricted in scale to some fraction of the distance to the surface. This means that the energetic eddies close to the wall are small, turbulent energy is added at high wavenumbers and a classical inertial range is unlikely to exist [7].

The considerations that have been made above on wall bounded flows are directly connected to the necessity of any computational method to resolve the near-wall flow field to capture correctly the mechanisms of production of turbulence. In the next section we will define the scales at which the near wall fluctuations take place to motivate the need to model the near wall region in a suitable way.

3 Channel flow

In this section we consider a turbulent flow through a rectangular duct of height $2h$ [19]. The mean flow is predominantly in the axial direction.

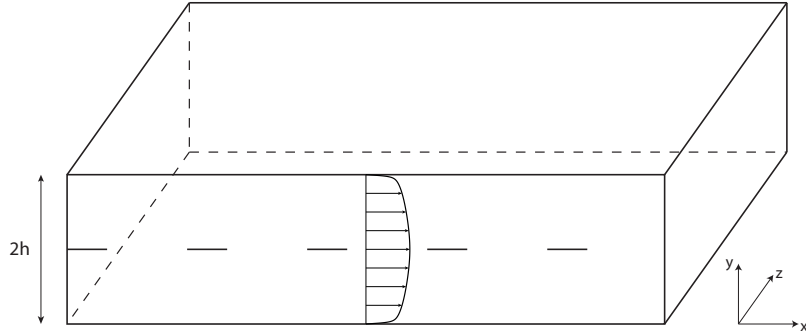


Figure 2: Sketch of channel flow

The following hypothesis are considered:

- The extent of the channel in the spanwise direction z is large compared to h so that the flow is statistically independent of z .
- The length of the channel is considerable with respect to its height so that the flow is fully developed at large x , hence it's statistically independent of x .
- The flow is statistically stationary.

We analyze the problem of a channel flow with a constant pressure gradient

$$\frac{dp}{dx} = a < 0 \quad (3.1)$$

the Reynolds number of the problem is

$$Re = \frac{\rho U_b 2h}{\mu} \quad (3.2)$$

where $U_b = 1/S \int_S U dS$ is the mean velocity along the section. The mean velocities in the three coordinate directions are (U, V, W) with fluctuations (u, v, w) and the mean pressure is also indicated with the capital P . The mean cross-stream velocity W is zero.

3.1 RANS equations of channel flow

Considering the continuity and momentum equations in the Reynolds Averaged Navier-Stokes formulation we get

$$\begin{cases} \vec{\nabla} \cdot \vec{U} = 0 \\ \rho \left(\frac{\partial \vec{U}}{\partial t} + \vec{U} \cdot \vec{\nabla} \vec{U} \right) = -\vec{\nabla} \vec{P} + \vec{\nabla} \cdot 2\mu \vec{\vec{E}} - \rho \vec{\nabla} \cdot \langle \vec{u}\vec{u} \rangle \end{cases} \quad (3.3)$$

where $\vec{\vec{E}} = \frac{\vec{\nabla} \vec{U} + \vec{\nabla} \vec{U}^T}{2}$.

Following the hypothesis listed above ($V = 0, \frac{\partial}{\partial x} = \frac{\partial}{\partial z} = \frac{\partial}{\partial t} = 0$), the mean continuity equation reduces to

$$\frac{dV}{dy} = 0 \quad (3.4)$$

since W is zero and U is independent of x . Considering the fact that V is zero at the wall, this implies that V needs to be zero in the entire domain, so we get $V = 0$.

The lateral mean momentum equation (y direction) reduces to

$$\frac{\partial P}{\partial y} - \rho \frac{\partial}{\partial y} \langle v^2 \rangle = 0 \quad (3.5)$$

which, with the boundary condition $\langle v^2 \rangle_{y=0} = 0$, integrates to

$$P - \rho \langle v^2 \rangle = P_w(x) \quad (3.6)$$

where $P_w(x)$ is the mean pressure at the wall. Taking the x derivative on both sides of equation (3.6) we get

$$\frac{\partial P}{\partial x} = \frac{dP_w}{dx} \quad (3.7)$$

that implies that the mean axial pressure gradient is uniform across the flow.

With this result (3.7) we can rewrite the axial mean momentum equation as

$$\frac{dP_w}{dx} = \frac{\partial}{\partial y} \left[\mu \frac{dU}{dy} - \rho \langle uv \rangle \right] \quad (3.8)$$

where we can see that the expression inside square brackets is a shear stress $\tau(y)$, that accounts for both viscous and Reynolds stress (additional stress caused by turbulence). Since the left hand side of equation (3.8) is a function of x while the right hand side is a function of y , to satisfy the equation both quantities need to be constant

$$\frac{\partial \tau}{\partial y} = \text{const} = a = \frac{dP_w}{dx} \quad (3.9)$$

that, with the boundary condition $\tau(0) = \tau(2h) = \tau_w$, integrates to

$$\tau(y) = \tau_w \left(1 - \frac{y}{h} \right) \quad (3.10)$$

that implies that the shear stress is a linear function of y .

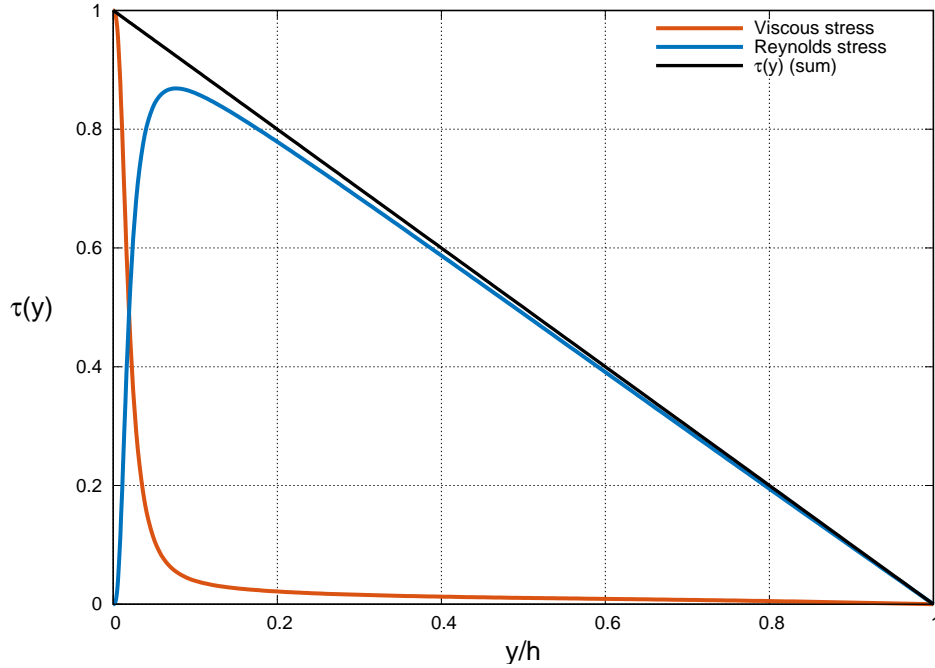


Figure 3: Profiles of the viscous shear stress ($\mu \frac{dU}{dy}$) and the Reynolds shear stress ($\rho \langle uv \rangle$) in turbulent channel flow: DNS data of Vreman [23]: $Re = 590$

We can also define a skin-friction coefficient as

$$C_f = \frac{\tau_w}{\frac{1}{2} \rho U_B^2} \quad (3.11)$$

We can observe that the pressure gradient is balanced exactly with the shear stress gradient at the wall

$$\frac{\partial \tau}{\partial y} = -\frac{\tau_w}{h} = \frac{\partial P_w}{\partial x} \quad (3.12)$$

Considering Figure 3 we can observe that the viscous stress dominates at the wall, a feature of wall bounded flows that is not present in free shear flows. Also, near the wall, since the viscosity is an influential parameter, the velocity profile depends upon the Reynolds number (again in contrast to free shear flows). It's useful to define near the wall some parameters using the density ρ , viscosity μ and wall shear stress τ_w . From this quantities we can define the friction velocity

$$u_\tau = \sqrt{\frac{\tau_w}{\rho}} \quad (3.13)$$

the viscous lengthscale

$$\delta_\nu = \frac{\nu}{u_\tau} \quad (3.14)$$

and the friction Reynolds number

$$Re_\tau = \frac{u_\tau h}{\nu} = \frac{h}{\delta_\nu} \quad (3.15)$$

From this quantities we can scale the velocity and wall distance as

$$U^+ = \frac{U}{u_\tau} \quad (3.16)$$

$$y^+ = \frac{y}{\delta_\nu} \quad (3.17)$$

This scaling is effective in bringing out the velocity variation near the wall

$$\left. \frac{dU^+}{dy^+} \right|_{y=0} = \frac{\delta_\nu}{u_\tau} \left. \frac{dU}{dy} \right|_{y=0} = \frac{\nu}{u_\tau} \frac{\tau_w}{\mu} = 1 \quad (3.18)$$

3.2 Mean velocity profiles

We can define different regions on the basis of y^+

- Viscous wall region ($y^+ < 50$): there is direct effect of molecular viscosity on the shear stress.
- Outer layer ($y^+ > 50$): the direct effect of viscosity is negligible.

Within the viscous wall region we can define the viscous sublayer ($y^+ < 5$), where the Reynolds shear stress is negligible compared with the viscous stress. Using the Taylor-series expansion we can determine the velocity profile in this region

$$U^+(y^+) = U^+|_{y^+=0} + \left. \frac{dU^+}{dy^+} \right|_{y^+=0} y^+ + O(y^+) \quad (3.19)$$

and since we have demonstrated in equation (3.18) that the velocity gradient near the wall is unitary we can write

$$U^+ = y^+ + O(y^+) \quad , \quad y^+ < 5 \quad (3.20)$$

that is the *law of the wall*.

Fully developed channel flow is completely specified by ρ , ν , h , u_τ or, equivalently, ρ , ν , h , $\frac{dP_w}{dx}$ since

$$u_\tau = \left(-\frac{h}{\rho} \frac{dP_w}{dx} \right) \quad (3.21)$$

From this quantities there are two non-dimensional parameters that can be defined: $\frac{y}{h}$ and $\frac{y}{\delta_\nu}$ (where the first refers to the outer layer and the second to the viscous region). From these parameters we can write the velocity gradient as

$$\frac{dU}{dy} = \frac{u_\tau}{y} \Phi \left(\frac{y}{h}, \frac{y}{\delta_\nu} \right) \quad (3.22)$$

Prandtl [20] postulated that, at high Reynolds number, near the wall ($y/h \ll 1$) there is an inner layer which is essentially independent of h , so in we can write

$$\frac{dU}{dy} = \frac{u_\tau}{y} \Phi \left(\frac{y}{\delta_\nu} \right) \quad (3.23)$$

whereas in the outer layer ($y/\delta_\nu \gg 1$)

$$\frac{dU}{dy} = \frac{u_\tau}{y} \Phi\left(\frac{y}{h}\right) \quad (3.24)$$

At the boundary between these two regions we can write

$$\lim_{y/\delta_\nu \gg 1} \frac{u_\tau}{y} \Phi\left(\frac{y}{\delta_\nu}\right) = \lim_{y/h \ll 1} \frac{u_\tau}{y} \Phi\left(\frac{y}{h}\right) = \frac{1}{\kappa} \quad (3.25)$$

hence in this region Φ has to be a constant that takes the values of $1/\kappa$, where κ is the von Kármán constant.

Thus, in this region, the mean velocity gradient is

$$\frac{dU}{dy} = \frac{u_\tau}{y} \frac{1}{\kappa} \quad (3.26)$$

that with the viscous scaling becomes

$$\frac{dU^+}{dy^+} = \frac{1}{\kappa y^+} \quad (3.27)$$

which integrates to

$$U^+ = \frac{1}{\kappa} \ln y^+ + B \quad (3.28)$$

where B is a constant. Equation (3.28) is the *log law*, that is in agreement with experimental results for $y^+ > 30$. Generally the two constants of the law are taken as

$$\kappa = 0.41 \quad , \quad B = 5.2 \quad (3.29)$$

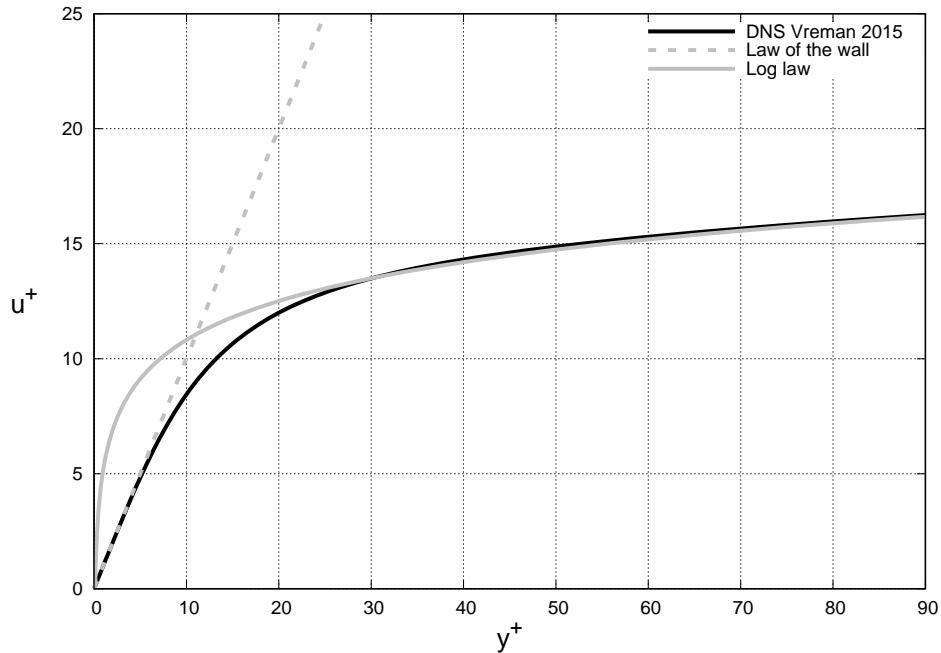


Figure 4: Near wall profiles of mean velocity: DNS data of Vreman [23]: $Re = 590$

The region between the viscous sublayer ($y^+ < 5$) and the log-law region ($y^+ > 30$) is called the buffer layer. It is the transition region between the viscosity-dominated and the turbulence-dominated parts of the flow.

3.3 Reynolds stresses

Analyzing the Reynolds stresses we can clearly see that in the viscous wall region ($y^+ < 50$) there is the most vigorous turbulent activity, whereas in the log-law region they are essentially uniform.

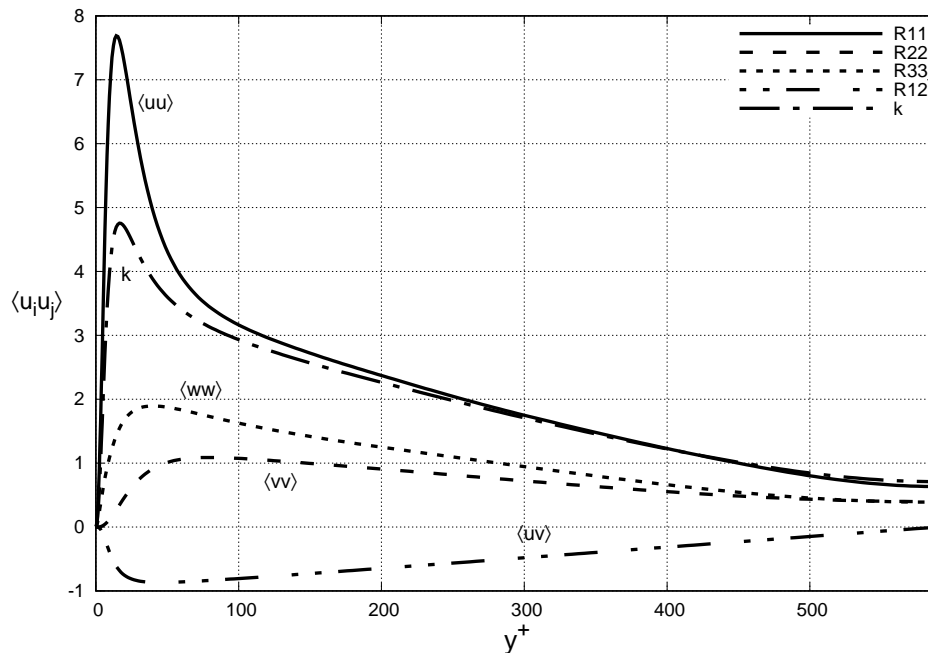


Figure 5: Reynolds stresses and kinetic energy against y^+ : DNS data of Vreman [23]: $Re = 590$

This consideration implies the need to resolve in detail the viscous wall region, but happens to be in contrast with how the viscous lengthscale varies with the Reynolds number. We have showed before that the lengthscale ratio is measured by the friction Reynolds number Re_τ , which increases almost linearly with Re (approximately $Re_\tau \approx 0.09Re^{0.88}$). Consequently, at high Reynolds number the viscous lengthscale can be vary small, thus imposing a real challenge both in simulating and physically measuring the flow.

3.4 Turbulent kinetic energy budget

Considering the balance equation for turbulent kinetic energy for a fully developed channel flow

$$0 = P - \tilde{\epsilon} + \nu \frac{d^2 k}{dy^2} - \frac{d}{dy} \left\langle \frac{1}{2} \nu \mathbf{u} \cdot \mathbf{u} \right\rangle - \frac{1}{\rho} \frac{d}{dy} \langle \nu p' \rangle \quad (3.30)$$

where in order the terms are production, pseudo-dissipation, viscous diffusion, turbulent convection, and pressure transport. It can be shown that the peak production occurs

precisely where the viscous stress and the Reynolds shear stress are equal, around $y^+ \approx 12$ (see Figure 24). At this location Production exceeds dissipation ($P/\epsilon \approx 1.8$), and the excess energy produced is transported from turbulent convection both toward the wall and in the log-law region. Viscous transport carries kinetic energy all the way to the wall, where occurs the peak dissipation through viscosity:

$$\epsilon = \tilde{\epsilon} = \nu \frac{d^2 k}{dy^2} \quad , \quad \text{for } y = 0 \quad (3.31)$$

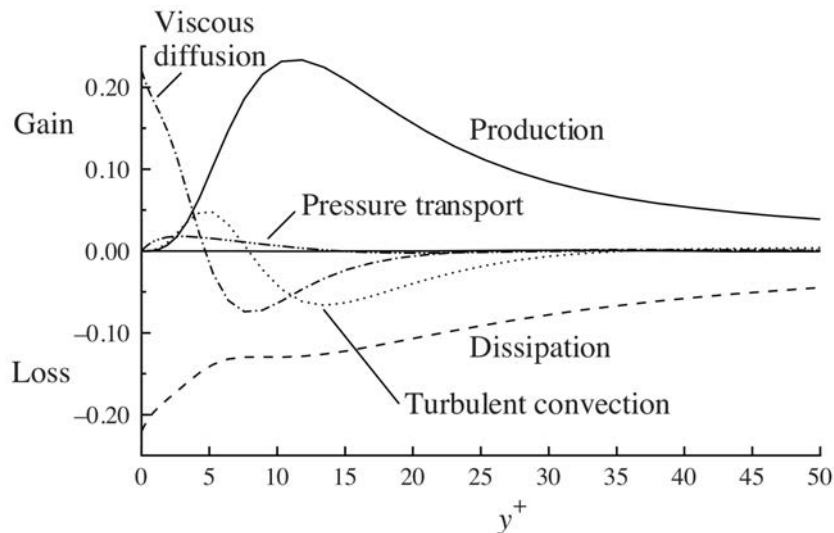


Figure 6: The turbulent kinetic energy budget in the viscous wall region of channel flow (Turbulent flows, Pope [19])

4 Computational fluid dynamics

In fluid dynamics, especially for turbulent flows, the large eddy simulation (LES) technique has become more and more widespread in the academic world for its ability to represent the non-stationary and multiscale nature of turbulence, essentially replacing the Reynolds-averaged Navier Stokes (RANS) approach. Infact the need to describe with relative accuracy non-stationary phenomena is inherently impossible to satisfy with RANS approach, that moreover has the problem of being non universal (it takes as input some constants that depend on the particular analyzed flow). The LES approach is conceptually more advanced than RANS, laying its foundations on the hypothesis of the Kolmogorov's K41 theory (2.1) where the fundamental hypothesis is that while the larger scale turbulent motions depends on the particular flow geometry, the smallest scales show an universal behaviour that doesn't depend on the type of flow analyzed. So the underlying idea of LES technique is to solve the Navier-Stokes equation for a filtered velocity field $\bar{U}(\mathbf{x}, t)$ which is representative of the larger-scale turbulent motions, including in the equations a model for the influence of the smaller-scale motions. These approaches are usually benchmarked using the Direct Numerical Simulation (DNS), that consists in directly discretizing the Navier-Stokes system of equations without introducing any model for turbulence.

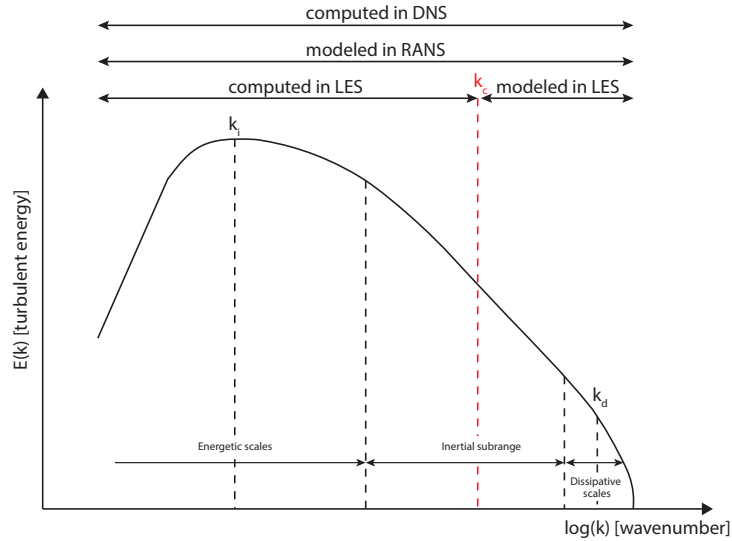


Figure 7: Turbulent energy spectrum with indications of the modeling introduced by LES, RANS and DNS. k_c is the wavenumber at which it's introduced the LES filter

4.1 Compressible Large eddy simulation

The Large eddy simulation approach requires four main conceptual steps:

- Define a filtering operator G_Δ to decompose the velocity into the sum of a filtered and a residual (or subgrid-scale, SGS) component. The filtered velocity field represents the motion of the large eddies while the residual component represents the small modeled scales.
- Apply the filtering operator to the Navier-Stokes equations to obtain the evolution of the filtered velocity field.
- Modeling the residual-stress tensor T_{ij}^{SGS} and the residual energy E_{ij}^{SGS} to obtain closure
- Solve numerically the filtered equations, which provides an approximation to the large-scale motions in one realization of the turbulent flow.

Being $\bar{\phi}$ a filtered flow variable, we define $\tilde{\phi}$ the Favre filter of ϕ as

$$\tilde{\phi} = \frac{\overline{\rho\phi}}{\bar{\rho}} \quad (4.1)$$

The filtered compressible non-dimensional Navier-Stokes equations, taking into account the definition (4.1) are (following the notation of Garnier et al. [8])

$$\left\{ \begin{array}{l} \frac{\partial \bar{p}}{\partial t} = -\frac{\partial \bar{\rho} \tilde{u}_j}{\partial x_j} \\ \frac{\partial \bar{\rho} \tilde{u}_i}{\partial t} = -\frac{\partial}{\partial x_j} (\bar{\rho} \tilde{u}_i \tilde{u}_j + \bar{p}_i \delta_{ij}) + \frac{\sqrt{\gamma} M_\infty}{Re} \frac{\partial}{\partial x_j} (\bar{\mu} \bar{d}_{ij}) - \frac{\partial}{\partial x_j} (\overline{\rho u_i u_j} - \bar{\rho} \tilde{u}_i \tilde{u}_j) \\ \frac{\partial \bar{\rho} \tilde{E}}{\partial t} = -\frac{\partial}{\partial x_j} ((\bar{\rho} \tilde{E} + \tilde{p} \tilde{u}_j)) \\ \quad + \frac{\sqrt{\gamma} M_\infty}{Re} \left(\frac{\gamma}{\gamma-1} \frac{1}{Pr} \frac{\partial}{\partial x_j} \left(k \frac{\partial \tilde{T}}{\partial x_j} \right) + \frac{\partial}{\partial x_j} (\bar{\mu} \bar{d}_{ij} \tilde{u}_i) \right) - \frac{\partial}{\partial x_j} \left(\overline{(\rho E + p) u_i} - (\bar{\rho} \tilde{E} + \tilde{p}) \tilde{u}_i \right) \end{array} \right. \quad (4.2)$$

where

$$d_{ij} = \mu \left(\frac{\partial u_i}{\partial x_j} + \frac{\partial u_j}{\partial x_i} - \frac{2}{3} \frac{\partial u_s}{\partial x_s} \delta_{ij} \right) \quad (4.3)$$

Comparing the filtered NS equations to the non filtered formulation we recognise two important contributions, expressed by

$$\bar{T}_{ij}^{SGS} = \overline{\rho u_i u_j} - \bar{\rho} \tilde{u}_i \tilde{u}_j \quad (4.4)$$

which is the subgrid-scale (SGS) stress tensor, and

$$\bar{E}_j^{SGS} = \overline{(\rho E + p) u_i} - (\bar{\rho} \tilde{E} + \tilde{p}) \tilde{u}_i \quad (4.5)$$

$$= \overline{\rho c_p T u_j} - \bar{\rho} \tilde{c}_p \tilde{T} \tilde{u}_j + \frac{1}{2} \bar{T}_{ij}^{SGS} \tilde{u}_j - \frac{1}{2} \bar{T}_{kk}^{SGS} \tilde{u}_j \quad (4.6)$$

which is the subgrid-scale energy term.

Equations (4.4) and (4.6) represent the under resolved turbulent contributions due to the filtering process that needs to be modeled in a suitable way.

Following the Boussinesq's hypothesis, the deviatoric part of the subgrid-scale stress tensor \bar{T}_{ij}^{SGS} can be written as

$$\bar{T}_{ij}^{SGS} - \frac{1}{3} \bar{T}_{kk}^{SGS} \delta_{ij} = -2\mu_{SGS} \left(\tilde{S}_{ij} - \frac{1}{3} S_{kk} \delta_{ij} \right) \quad (4.7)$$

where μ_{SGS} is the subgrid eddy viscosity, \bar{T}_{kk}^{SGS} is the isotropic contribution to the subgrid stress tensor and \tilde{S}_{ij} denotes the resolved strain-rate tensor

$$\tilde{S}_{ij} = \frac{1}{2} \left(\frac{\partial \tilde{u}_i}{\partial x_j} + \frac{\partial \tilde{u}_j}{\partial x_i} \right) \quad (4.8)$$

In the same way, the energy subgrid-scale terms are modeled as

$$\bar{E}_j^{SGS} = -\lambda_{SGS} \frac{\partial \tilde{T}}{\partial x_j} + \frac{1}{2} \bar{T}_{ij}^{SGS} \tilde{u}_j - \frac{1}{2} \bar{T}_{kk}^{SGS} \tilde{u}_j \quad (4.9)$$

where λ_{SGS} is the subgrid-scale turbulent diffusivity expressed by

$$\lambda_{SGS} = \mu_{SGS} \frac{\bar{c}_p}{Pr_T} \quad (4.10)$$

in which $Pr_T = 0.9$ is the turbulent Prandtl number. Collecting the viscosity from both resolved and subgrid scales in one term we get

$$\bar{\mu}_{tot} = \mu(\tilde{T}) + \frac{Re}{\sqrt{\gamma}M} \mu_{SGS} \quad (4.11)$$

and doing the same for the turbulent diffusivity

$$\bar{\lambda}_{tot} = \frac{\gamma}{\gamma - 1} \left(\frac{\mu(\tilde{T})}{Pr} + \frac{Re}{\sqrt{\gamma}M} \frac{\mu_{SGS}}{Pr_T} \right) \quad (4.12)$$

we can now write the filtered Navier Stokes equations with the Bousinessq's hypothesis

$$\begin{cases} \frac{\partial \bar{p}}{\partial t} = -\frac{\partial \bar{\rho} \tilde{u}_j}{\partial x_j} \\ \frac{\partial \bar{\rho} \tilde{u}_i}{\partial t} = -\frac{\partial}{\partial x_j} (\bar{\rho} \tilde{u}_i \tilde{u}_j + \bar{p}_i \delta_{ij}) + \frac{\sqrt{\gamma} M_\infty}{Re} \frac{\partial}{\partial x_j} (\bar{\mu}_{tot} \bar{d}_{ij}) \\ \frac{\partial \bar{\rho} \tilde{E}}{\partial t} = -\frac{\partial}{\partial x_j} ((\bar{\rho} \tilde{E} + \tilde{p} \tilde{u}_j)) + \frac{\sqrt{\gamma} M_\infty}{Re} \left(\bar{\lambda}_{tot} \frac{\partial}{\partial x_j} \left(k \frac{\partial \tilde{T}}{\partial x_j} \right) + \frac{\partial}{\partial x_j} (\bar{\mu} \bar{d}_{ij} \tilde{u}_i) \right) \end{cases} \quad (4.13)$$

From set of equations (4.13) we can see that the filtering process, in combination with the Bousinessq hypotesis, intruduces a further unknown (μ_{SGS}). The required model for μ_{SGS} needs to universal and exploitable in a wide range of flow situations, thus is the focal point of LES which is still in study by the turbulence community. The most exploited model for turbulent eddy viscosity is purely algebraic and reduces to the expression

$$\mu_{SGS} = \bar{\rho} (C_m \Delta)^2 D_m [\bar{\mathbf{U}}] \quad (4.14)$$

where C_m is a tuning parameter, $\Delta = (\Delta x \Delta y \Delta z)^{1/3}$ is the subgrid characteristic lenght expressing the size of the filter and $D_m [\cdot]$ is the non-linear differential operator of the model applied to the resolved flow quantities $\bar{\mathbf{U}}$. In this thesis the model taken into account is the *Wall-Adaptive Large-Eddy* (WALE) which is described below.

4.2 The wall-adaptive Large-Eddy viscosity model

According to Nicoud and Ducros [18], who found a model which exhibit the asymptotic behaviour of $\mu_{SGS} \sim O(y^+)^3$ in the near wall region (which is not respected in the Smagorinsky model for example), the non-linear differential operator can be defined as

$$D_W [\bar{\mathbf{U}}] = \frac{(S_{ij}^d S_{ij}^d)^{3/2}}{(S_{ij}^d S_{ij}^d)^{5/2} + (S_{ij}^d S_{ij}^d)^{5/4}} \quad (4.15)$$

where S_{ij}^d is the traceless symmetric part of the square of the resolved velocity gradient tensor, defined as

$$S_{ij}^d = \frac{1}{2} \left(\frac{\partial \tilde{u}_i}{\partial x_l} \frac{\partial \tilde{u}_l}{\partial x_j} + \frac{\partial \tilde{u}_j}{\partial x_l} \frac{\partial \tilde{u}_l}{\partial x_i} \right) - \frac{1}{3} \frac{\partial \tilde{u}_m}{\partial x_l} \frac{\partial \tilde{u}_l}{\partial x_m} \delta_{ij} \quad (4.16)$$

The constant $C_W = 0.325$ is found by statistical correlations based on DNS benchmarks. The WALE model also possesses the interesting property that μ_{SGS} vanishes if the flow is two-dimensional, in agreement with the physical behaviour.

5 WMLES overview

The filtering of the unknowns used in LES leads to the cost of simulation being significantly less than that of DNS. However, the problem that arise in bounded flows is that in the inner part of the boundary layers is generated the peak production of turbulence, that from the smaller scales is carried to the largest ones. If the resolution of the grid cannot represent the inner-layer dynamics (production, dissipation, streaks, etc.), which is often the case for high Reynolds number LES simulations to reduce the computational cost, the resolved outer-layer turbulence cannot be regarded as a representation of reality. This problem is often referred to as the near-wall problem of LES and it becomes greater as the Reynolds number increases, because the scale of the inner layer dynamics decreases (see section 3.3). The wall-modeled large eddy simulation (WMLES) approach is to model the energetic eddies in the near-wall inner layer, this can be done in a variety of ways that are represented by the two following categories:

- **Hybrid LES/RANS:** LES is defined above a certain distance h_{wall} from the wall, while the near-wall region is modeled with RANS equations.
- **Wall-stress models:** LES is defined all the way to the wall, but since it doesn't resolve the inner-layer dynamics, takes as boundary conditions the shear stress τ_{wall} and the heat flux q_{wall} computed with a simplified set of equations solved in a independent grid.

Since this thesis is concerned with the implementation of a particular type of wall-stress model, we will first analyze the different possible approaches before going in the details of theory and implementation of an ordinary differential equation (ODE) based wall-stress model.

5.1 Wall stress models

Most wall-stress models are based on the physical principle of momentum conservation in a nearly parallel shear flow. Since the objective is to avoid resolving any turbulence in the inner layer, wall-model equations must be written assuming that the flow is on average aligned with the streamwise direction. According to Larsson et al.[12] the filtered momentum conservation equation assuming the special case of uniform-density flow aligned (on average) with the x direction (often referred as turbulent boundary layer equation, TBLE) results

$$\frac{\partial u}{\partial t} + \frac{\partial uu_j}{\partial x_j} + \frac{1}{\rho} \frac{\partial p}{\partial x} = \frac{\partial}{\partial y} \left[(\nu + \nu_{t,wm}) \frac{\partial u}{\partial y} \right] \quad (5.1)$$

where the eddy-viscosity is often given by a zero-equation mixing-length model like

$$\nu_{t,wm} = \kappa u_\tau y [1 - \exp(-y^+/A^+)]^2 \quad (5.2)$$

which is derived by Yang et al. [24].

In equation (5.2) $\kappa = 0.41$ is the Von Kàrman constant, $u_\tau = \sqrt{\tau_w/\rho}$ is the friction velocity, $y^+ = (u_\tau y/\nu_w)$ is the wall unit and $A^+ = 17$ is a constant of the Van Driest dumping function, which is

$$D = [1 - \exp(-y^+/A^+)]^2 \quad (5.3)$$

Equation (5.1) can be simplified with the equilibrium model, where it's assumed that the convection and the pressure-gradient balance exactly, thus the left hand side of eq. (5.1) becomes zero. The resulting ODE has the solution $u^+ \approx y^+$ for $y^+ \lesssim 5$ and $u^+ \approx \ln(y^+)/\kappa + B$ (log law) for $y^+ \gtrsim 30$. There are three main approaches to the implementation of a wall stress model:

- **Algebraic implementation**
- **Partial differential equations (PDE) implementation**
- **Ordinary differential equations (ODE) implementation**

in which the Algebraic and ODE implementation take advantage of the equilibrium model, whereas the PDE implementation does not and tries to solve the complete TBLE (5.1).

5.1.1 Algebraic implementation

Algebraic models were the first to be developed, being the simplest. Considering the log-law (3.28), we can rewrite it as

$$\frac{\langle u \rangle}{u_\tau} - \frac{1}{\kappa} \ln \left(\frac{y u_\tau}{\nu} \right) - B = 0 \quad (5.4)$$

where is worth remembering that $u_\tau = \sqrt{\tau_w/\rho}$. If an approximation of $\langle u \rangle$ can be obtained from the LES solution at the sampling point ($y = h_{wm}$) which should be placed in the log-layer, the above expression constitutes a non-linear algebraic equation for the unknown mean wall shear stress $\langle \tau_w \rangle$ which can be solved using an iterative procedure (e.g. Newton-Raphson method). The computed $\langle \tau_w \rangle$ is then enforced at the wall as a boundary condition. It's clear that the advantage of the algebraic implementation is that it requires much lesser computational cost, but the major drawback is the incorrect modelling of the wall attached eddies that normally dominate transfer mechanisms in the inertial layer [7].

5.1.2 PDE implementation

The PDE-based wall stress model requires that the full turbulent boundary layer equations (TBLE) are solved, which are presented in equation (5.1). These equation should be solved on a separate three dimensional grid spanning the wall-normal distance between the wall and h_{wm} . The LES velocity and the pressure gradient (which can be assumed constant in the wall normal direction) at height h_{wm} serve as boundary condition and the filtered wall shear stress obtained from solving the TBLE is enforced at the wall of the LES domain. The TBLE have to be complemented by a RANS model for computing ν_t , that is often a simple one-dimensional turbulence model.

Despite the potential to be the most accurate type of wall-stress models, the TBLE-approach has some drawbacks, namely

- The complexity of implementation in a general purpose CFD solver
- Coupling the solution of two sets of PDEs in a parallel, unstructured setting is challenging

- The generation of the embedded grid is difficult to implement for arbitrary geometries
- The cost of WMLES becomes no longer independent of Re_τ , because the embedded grid has to be wall resolved in the wall-normal direction

In general, the insignificant amount of evidence regarding the superiority of these models compared to simpler approaches is a big factor in the choice of which wall stress model to use.

5.1.3 ODE implementation

An alternative to directly solving the TBLE expressed in equation (5.1) is assuming that the convection and the pressure-gradient balance exactly, thus the left hand side of eq.(5.1) becomes zero. This assumption is called the equilibrium model, which takes as inputs the instantaneous velocity, temperature and pressure from LES field at a chosen height h_{wall} (that should be placed in the log-layer) and gives as outputs the wall stress τ_{wall} and wall heat flux q_{wall} obtained by solving the momentum and total energy equations simplified using the equilibrium model.

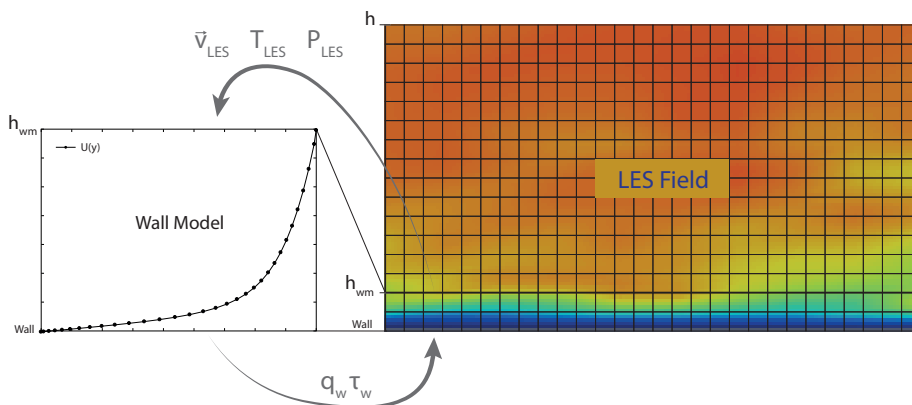


Figure 8: Coupling between LES and wall model

In this model the pressure is assumed to be wall-normal independent and the wall parallel velocity is calculated as $u_p = \sqrt{u^2 + w^2}$ (assuming $\vec{v} = (u, v, w)$). The two outputs τ_{wall} and q_{wall} are calculated using the parallel velocity and temperature gradients at the wall (a different approach to evaluate q_{wall} in high speed compressible flows is presented in section 5.2):

$$\tau_{wall} = \mu_w \left. \frac{du_p}{dy} \right|_{wall} \quad (5.5)$$

$$q_{wall} = \lambda_w \left. \frac{dT}{dy} \right|_{wall} \quad (5.6)$$

Compared to the Algebraic approach, the ODE implementation has the ability to account for other physical effects, such as strongly non-adiabatic compressible flow [12]. Another slight advantage of the ODE implementation is that it produces the right wall-stress even

when the grid locally approaches traditional LES resolution with resolved viscous and buffer layers.

The simplified momentum and total energy equations using the equilibrium model for compressible flow are (the capital U is the averaged wall parallel velocity):

$$\frac{d}{dy} \left[(\mu_{wm} + \mu_{t,wm}) \frac{dU_{wm}}{dy} \right] = 0 \quad (5.7)$$

$$\frac{d}{dy} \left[c_p \left(\frac{\mu_{wm}}{Pr} + \frac{\mu_{t,wm}}{Pr_{t,wm}} \right) \frac{dT_{wm}}{dy} \right] = - \frac{d}{dy} \left[(\mu_{wm} + \mu_{t,wm}) U_{wm} \frac{dU_{wm}}{dy} \right] \quad (5.8)$$

where c_p is the specific heat at constant pressure, Pr is the Prandtl number, $Pr_{t,wm} = 0.9$ is the turbulent Prandtl number (a model parameter) and the eddy-viscosity $\mu_{t,wm}$ is defined like equation (5.2)

$$\mu_{t,wm} = \kappa \rho_{wm} \sqrt{\frac{\tau_{w,wm}}{\rho_{wm}}} y [1 - \exp(-y^*/A^+)]^2 \quad (5.9)$$

$$y^* = \frac{u_\tau y}{\nu} \quad (5.10)$$

with the exception that the scaled wall distance y^* is in semi-local scaling (the dynamic viscosity changes along y) in order to work in strongly non-adiabatic conditions. Under the equilibrium assumption, the bracked quantities in eqs. (5.7) and (5.8) are constant across the wall-modeled layer. These conserved quantities correspond to the sum of the viscous and turbulent shear stress (in eq. (5.7)) and to the sum of molecular heat conduction, turbulent heat transport (left hand side of eq. (5.8)) and aerodynamic heating (right hand side of eq. (5.8)).

These equations need to be solved in an independent grid that goes from the wall to h_{wall} and can be stretched near the wall to increase the accuracy of the computation of τ_{wall} and q_{wall} .

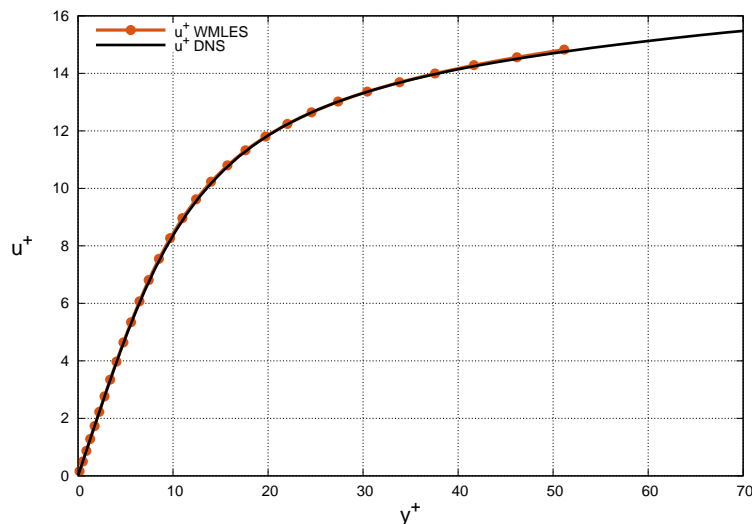


Figure 9: Example of the wall modelled mean velocity in ODE implementation compared to DNS data of Bernardini [14]: $M = 0.1$, $Re_\tau = 1000$

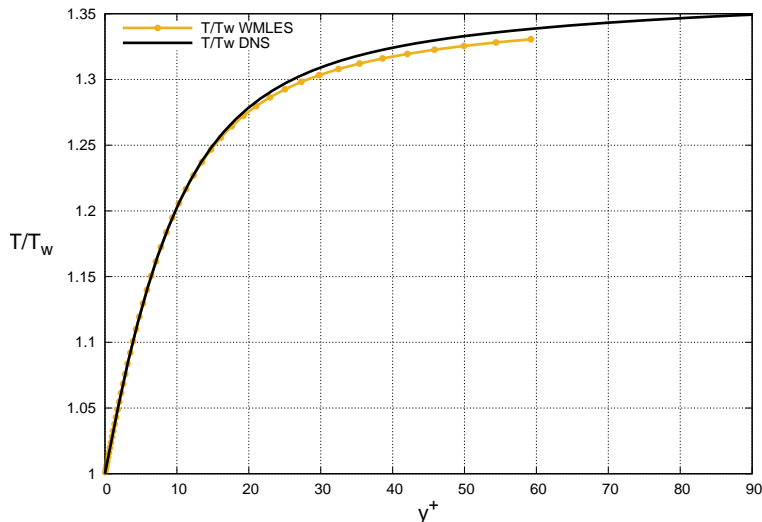


Figure 10: Example of the wall modelled mean temperature in ODE implementation compared to DNS data of Modesti [16]: $M = 1.5$, $Re_\tau = 500$

5.2 Further considerations on the Equilibrium Wall-Modeled Energy Equation

In the case of compressible flows the energy equation plays an essential role, thus it needs to be analyzed in more detail to understand what are the important quantities that regulate the heat flow and their importance in the near-wall region, which is the interest of WMLES. The energy equation (5.8) can be rewritten as

$$\frac{d}{dy} \left[(\mu_{wm} + \mu_{t,wm}) U_{wm} \frac{dU_{wm}}{dy} + c_p \left(\frac{\mu_{wm}}{Pr} + \frac{\mu_{t,wm}}{Pr_{t,wm}} \right) \frac{dT_{wm}}{dy} \right] = 0 \quad (5.11)$$

where the term $(\mu_{wm} + \mu_{t,wm}) U_{wm} dU_{wm}/dy$ represents the aerodynamic heating, the term $c_p \mu_{wm}/Pr dT_{wm}/dy$ the molecular heat of conduction and $c_p \mu_{t,wm}/Pr_{t,wm} dT_{wm}/dy$ the turbulent heat transport. The molecular heat conduction prevails over the turbulent heat transport close to the wall where $y^+ \ll (A^+)^{2/3}$ (see equation (5.9)). The opposite occurs relatively far away from the wall, when $y^+ \gg (A^+)^{2/3}$, where the ratio of molecular to eddy viscosities is small, $\mu/\mu_T \sim 1/(\kappa y^+) \ll 1$. According to [25] if we evaluate the first integral of the energy equation from 0 to h_{wall} we get

$$q_w = \left(U_{wm} \tau_w + c_p \frac{\mu_{t,wm}}{Pr_{t,wm}} \frac{dT}{dy} \right)_{y=h_{wall}} \quad (5.12)$$

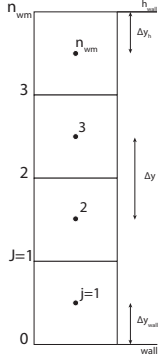
where the molecular heat has been neglected on the right hand side because $\mu/\mu_T = O(\delta_\nu/h_{wall}) \ll 1$. This equation states that the wall heat flux is the sum of aerodynamic heating and the turbulent heat transport at the matching location (h_{wall}), with each represented by the first and second terms on the right-hand side, respectively. This definition of q_w is useful also in adiabatic flows ($q_w = 0$) where the slope of the temperature at the edge of the wall-modeled layer is not necessarily zero in high speed conditions, where the aerodynamic heating becomes important because that extra heat must be evacuated to the bulk flow.

6 Discretization of the wall-stress model equations

In this section it's presented the finite volume discretization of equations (5.7) and (5.8). It's important to note that the velocity and temperature are located in the centroid of the cells while their coefficients are located in the faces. There is an exception for velocity and temperature at the wall and h_{wall} positions that are located respectively in the first and last face of the grid and accounted as boundary conditions to the non-linear system that the discretized equations represent, as it will become clear later.

6.1 Discretization of the momentum equation

In the following equations the index j indicates the j -th centroid, whereas the capital J indicates the J -th face, as shown in the figure below. Let's collect the sum of the molecular viscosity and turbulent viscosity in a coefficient $K_u = (\mu_{wm} + \mu_{t,wm})$. Considering a second order finite volume discretization for the momentum equation we get:



$$K_u^J \frac{U_{j+1} - U_j}{\Delta y_J} - K_u^{J-1} \frac{U_j - U_{j-1}}{\Delta y_{J-1}} = 0 \quad (6.1)$$

at the wall:

$$K_u^J \frac{U_{j+1} - U_j}{\Delta y_J} - K_u^{wall} \frac{U_j - U_{wall}}{\Delta y_{wall}} = 0 \quad (6.2)$$

and at h_{wall} :

$$K_u^h \frac{U_h - U_j}{\Delta y_h} - K_u^{J-1} \frac{U_j - U_{j-1}}{\Delta y_{J-1}} = 0 \quad (6.3)$$

These equations represent the following tri-diagonal system, written for this simplified case of an uniform grid with four cells:

$$\begin{bmatrix} -\bar{K}_u^J - \bar{K}_u^{wall} & \bar{K}_u^J & 0 & 0 \\ \bar{K}_u^{J-1} & -\bar{K}_u^{J-1} - \bar{K}_u^J & \bar{K}_u^{J+1} & 0 \\ 0 & \bar{K}_u^{J-1} & -\bar{K}_u^{J-1} - \bar{K}_u^J & \bar{K}_u^{J+1} \\ 0 & 0 & \bar{K}_u^{J-1} & -\bar{K}_u^J - \bar{K}_u^h \end{bmatrix} \begin{bmatrix} U_1 \\ U_2 \\ U_3 \\ U_4 \end{bmatrix} = \begin{bmatrix} -\bar{K}_u^{wall} \\ 0 \\ 0 \\ -\bar{K}_u^h \end{bmatrix} \quad (6.4)$$

where it's been made the substitution $\bar{K}_u^J = K_u^J / \Delta y_J$ to simplify the reading.

6.2 Discretization of the total energy equation

As before let's introduce a coefficient that simplify the equations: $K_T = c_p \left(\frac{\mu_{wm}}{Pr} + \frac{\mu_{t,wm}}{Pr_{t,wm}} \right)$. Considering a second order finite volume discretization for the total energy equation we get:

$$\begin{aligned}
& K_T^J \frac{T_{j+1} - T_j}{\Delta y_J} - K_T^{J-1} \frac{T_j - T_{j-1}}{\Delta y_{J-1}} = \\
& - \left[K_u^J \frac{U_{j+1} + U_j}{2} \frac{U_{j+1} - U_j}{\Delta y_J} - K_u^{J-1} \frac{U_j + U_{j-1}}{2} \frac{U_j - U_{j-1}}{\Delta y_{J-1}} \right]
\end{aligned} \tag{6.5}$$

at the wall:

$$\begin{aligned}
& K_T^J \frac{T_{j+1} - T_j}{\Delta y_J} - K_T^{wall} \frac{T_j - T_{wall}}{\Delta y_{wall}} = \\
& - \left[K_u^J \frac{U_{j+1} + U_j}{2} \frac{U_{j+1} - U_j}{\Delta y_J} - K_u^{wall} U_{wall} \frac{U_j - U_{wall}}{\Delta y_{wall}} \right]
\end{aligned} \tag{6.6}$$

and at h_{wall} :

$$\begin{aligned}
& K_T^h \frac{T_h - T_j}{\Delta y_h} - K_T^{J-1} \frac{T_j - T_{j-1}}{\Delta y_{J-1}} = \\
& - \left[K_u^h U_h \frac{U_h - U_j}{\Delta y_h} - K_u^{J-1} \frac{U_j + U_{j-1}}{2} \frac{U_j - U_{j-1}}{\Delta y_{J-1}} \right]
\end{aligned} \tag{6.7}$$

These equations represent the following tri-diagonal system, written for this simplified case of an uniform grid with four cells:

$$\begin{bmatrix}
-\bar{K}_T^J - \bar{K}_T^{wall} & \bar{K}_T^J & 0 & 0 \\
\bar{K}_T^{J-1} & -\bar{K}_T^{J-1} - \bar{K}_T^J & \bar{K}_T^{J+1} & 0 \\
0 & \bar{K}_T^{J-1} & -\bar{K}_T^{J-1} - \bar{K}_T^J & \bar{K}_T^{J+1} \\
0 & 0 & \bar{K}_T^{J-1} & -\bar{K}_T^J - \bar{K}_T^h
\end{bmatrix}
\begin{bmatrix}
T_1 \\
T_2 \\
T_3 \\
T_4
\end{bmatrix}
=
\begin{bmatrix}
rhs_{wall} \\
0 \\
0 \\
rhs_h
\end{bmatrix} \tag{6.8}$$

where it's been made the substitution $\bar{K}_T^J = K_T^J / \Delta y_J$ to simplify the reading and rhs_{wall} and rhs_h represents the known right hand sides of equations (6.6) and (6.7).

Given the fact that momentum and total energy equations are coupled, they represent a ODE-system that can to be solved in a segregated fashion:

1. Solve the momentum equation treating μ_{wm} and $\mu_{t,wm}$ as fixed
2. Update $\tau_{w,wm}$ and $\mu_{t,wm}$
3. Solve the energy equation while treating everything except T_{wm} as fixed
4. Update $\tau_{w,wm}$, μ_{wm} , ρ_{wm} and $\mu_{t,wm}$
5. Repeat until converge (measured by the values of $\tau_{w,wm}$ and q_{wall})

The values of $\tau_{w,wm}$ and $q_{w,wm}$ are computed using the velocity and temperature at the first node of the wall model grid:

$$\tau_{w,wm} = \mu_w \frac{U_1 - U_{wall}}{\Delta y_{wall}} \tag{6.9}$$

$$q_{w,wm} = \lambda_w \frac{T_1 - T_{wall}}{\Delta y_{wall}} \tag{6.10}$$

Since both equations are in practice a tridiagonal system they can be solved efficiently by the tri-diagonal matrix algorithm (TDMA). This algorithm has been implemented in

Fortran 90 as a subroutine of the numerical solver Unsteady Robust All-around Navier-Stokes Solver (URANOS) [5] [6] [22], which has been realized by my supervisor (prof. Francesco De Vanna) during his PhD with the purpose of the fluid simulation of compressible viscous flows capable of dealing with moving bodies at high-Mach numbers with high order accuracy and high resolution.

URANOS has been used to solve the filtered compressible Navier-Stokes equations (for the theoretical aspects see Garnier et al. (2009) [8]) and it has been chosen to use the Wall-Adaptive Large-Eddy (WALE) viscosity model (Nicoud and Ducros (1999) [18]) that is physically consistent to the wall-turbulence theory, which predicts a cubic behaviour in the wall-inner layer $\mu_{SGS} \approx O(y^+)^3$. This choice has been made to get acceptable results in both wall modeled and wall resolved configurations.

6.3 Numerical aspects of wall stress model

The ODE-system described in the previous section needs to be solved from $y = 0$ to $y = h_{wall}$. It has been chosen to use a lightly stretched finite volume grid defined by

$$y_{f,J} = \Delta y_w \frac{r^J - 1}{r - 1} \quad , \quad J = 0, 1, \dots, n_{wm} \quad (6.11)$$

where r is the stretching parameter and Δy_w is the spacing at the wall, that needs to be chosen accurately in order to have the first point around $y^+ \approx 1$. The centroids coordinates therefore result

$$y_{c,J} = \frac{y_{f,J} + y_{f,J+1}}{2} \quad , \quad J = 0, 1, \dots, n_{wm} - 1 \quad (6.12)$$

so consequently there will be n_{wm} coefficients on grid faces and $n_{wm} - 1$ velocities and temperatures on centroids. The choice of n_{wm} , r and $y^+ \approx 1$ is a trade-off between good resolution near the wall (i.e. acceptable error) and computational cost while limiting the stretching parameter.

6.4 Coupling LES to wall stress model

After solving both equations and reaching convergence with the desired tolerance remains the task to transfer the information of τ_{wall} and q_{wall} to LES field. At this stage it's worth pointing out that LES grid is uniform and boundary conditions are given using ghost nodes, which are as many as required by the order of finite differences used in the main code. To clarify the reading the following figure shows a LES grid with four ghost nodes that is coupled to a stretched wall-stress model grid at the second internal LES node, which is at h_{wm} height.

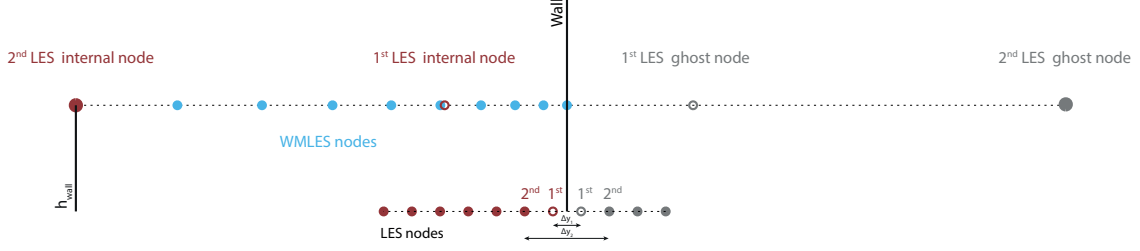


Figure 11: LES and wall-stress model grids combination

Since the information of τ_{wall} and q_{wall} has to be given to the internal domain by specifying velocities and temperatures in the ghost nodes a first approach would be to write equations (6.9) and (6.10) with a second order central finite difference for every ghost node, thus relating it with its symmetric internal node

$$\tau_{w,wm} = \mu_w \frac{U_i^{int} - U_i^{ghost}}{\Delta y_i} \quad (6.13)$$

$$q_{w,wm} = \lambda_w \frac{T_i^{int} - T_i^{ghost}}{\Delta y_i} \quad (6.14)$$

Solving (6.13) and (6.16) for U_i^{ghost} and T_i^{ghost} we get

$$U_i^{ghost} = U_i^{int} - \frac{\tau_{w,wm} \Delta y_i}{\mu_w} \quad (6.15)$$

$$T_i^{ghost} = T_i^{int} - \frac{q_{w,wm} \Delta y_i}{\lambda_w} \quad (6.16)$$

and with this condition we impose the right wall stress and wall heat flux to the internal domain. However this implementation tends to convergence problems because Δy_j tends to be very large due to the poor wall resolution of LES grid, resulting in a large negative value of U_i^{ghost} that leads to instability.

Another approach is to consider that every LES simulation has a model for the subgrid viscosity and thermal conductivity (e.g. Smagorinsky, WALE, etc.), that are specified in every point of the domain to bring the contribution of non resolved eddies. If we solve equations (6.13) and (6.16) for μ_{eff} and λ_{eff} (effective values) we can impose them to LES model at the wall using the values of τ_{wall} and q_{wall} computed with the wall stress model, instead of directly imposing them as boundary conditions

$$\mu_{eff} = \tau_{w,wm} \frac{\Delta y_i}{U_i^{int} - U_i^{ghost}} \quad (6.17)$$

$$\lambda_{eff} = q_{w,wm} \frac{\Delta y_i}{T_i^{int} - T_i^{ghost}} \quad (6.18)$$

where $q_{w,wm}$ is computed using equation (6.24). In the ghost nodes the required specification for velocity and temperature would be imposed using the no slip boundary condition for the former and the isothermal wall condition for the latter:

$$u_i^{ghost} = -u_i^{int} \quad (6.19)$$

$$v_i^{ghost} = -v_i^{int} \quad (6.20)$$

$$w_i^{ghost} = -w_i^{int} \quad (6.21)$$

$$T_i^{ghost} = 2T_w - T_i^{int} \quad (6.22)$$

This implementation has proven to be more stable in terms of convergence, but requires two corrections.

- If we look at equation (6.22), it's possible that the value of T_i^{ghost} is set in such a way that the temperature gradient $(T_i^{int} - T_i^{ghost})/\Delta y_i$ results negative (and consequently the λ_{eff} , eq. (6.18)), leading to convergence problems (this possibility is rare because in the channel the flow is on average hotter than the wall, resulting in a positive temperature gradient, but nevertheless a temporary colder configuration can happen). To avoid that we had to set $\lambda_{eff} = 0$ if it's negative. This problem is not encountered in the definition of μ_{eff} because the velocity gradient cannot be negative, given equation (6.19).
- Considering equations (6.17) and (6.18), if velocity and temperature gradients tends to zero at the wall, μ_w and λ_w tends to very high values to assure the right τ_{wall} and q_{wall} , but since a zero velocity or temperature gradient result in a zero τ_{wall} and q_{wall} we have to limit the viscosity and thermal conductivity to prevent them to be too large. In this implementation it was found that a maximum value of 30 for μ_{eff} and $30 \cdot c_p/Pr \approx 148$ for λ_{eff} (since $\lambda = \mu c_p/Pr$) leads to good results.

However, the simulation in the compressible case has proven to be considerably more challenging than the incompressible one because the heat generated inside the flow has to be dissipated in the correct way by the wall model. In particular we found that in our implementation computing the wall heat flux with equation (6.10) was leading to a continuous increase of the temperature of the channel, showing that the wall (which is cooler than the inside of the channel) was incapable to evacuate the heat generated by the flow, thus preventing it to heating up indefinitely. For this reason we looked if this problem was addressed in literature finding the expression of $q_{w,wm}$ from [25] that is derived in section 5.2 which is more suitable to high speed flows because even when the flow is instantaneously adiabatic $q_{w,wm}$ is not zero, therefore it is capable to still transfer some heat generated from the flow towards the outside. This implementation has proven to be more stable, succeeding to reach an equilibrium from the heat generated and dissipated that gives a stable temperature profile.

To sum up the discussion above our implementation is the following:

- Solve equations (5.7) and (5.8) obtaining the velocity and temperature profiles (convergence is reached when the variation of $\tau_{w,wm}$ and $q_{w,wm}$ computed with equations (6.9) and (6.10) is less than a given tolerance)
- Compute $\tau_{w,wm}$ and $q_{w,wm}$ as

$$\tau_{w,wm} = \mu_w \left. \frac{dU_{wm}}{dy} \right|_{wall} \quad (6.23)$$

$$q_{w,wm} = \left(U_{wm} \tau_{w,wm} + c_p \frac{\mu_{t,wm}}{Pr_{t,wm}} \frac{dT}{dy} \right)_{y=h_{wall}} \quad (6.24)$$

- Impose the boundary condition of μ_{eff} and λ_{eff} to the subgrid viscosity $VIS(i, j, k)$ and thermal conduction $LMD(i, j, k)$ as

$$VIS(i, jg, k) = 2\mu_{eff} - VIS(i, ji, k) \quad (6.25)$$

$$LMD(i, jg, k) = 2\lambda_{eff} - LMD(i, ji, k) \quad (6.26)$$

- Impose the no slip condition for velocity and the isothermal wall for temperature like in the wall resolved case (equations (6.19), (6.20), (6.21), (6.22))

This implementation has also the advantage that by increasing the number of points in the domain the WMLES progressively becomes a WRLES, so it's not an independent approach.

7 Simulation at Mach = 0.1

In this section are presented the results of the simulations computed with URANOS at various Reynolds numbers. The Mach number is set to 0.1 to avoid any compressible effects, thus the resulting driven pressure gradient is set equal to $\frac{d\langle p \rangle}{dx} = \sqrt{\gamma} M_\infty - u_b$. The channel sizes are $2\pi h \times 2h \times \pi h$ and the following boundary conditions are enforced to its faces:

- *Periodic boundary conditions* along the stream-wise and the span-wise directions
- *No-slip isothermal wall conditions* at the top and the bottom side of the domain (with wall temperature equal to $T/T_0 = 1$)

as shown in the figure below

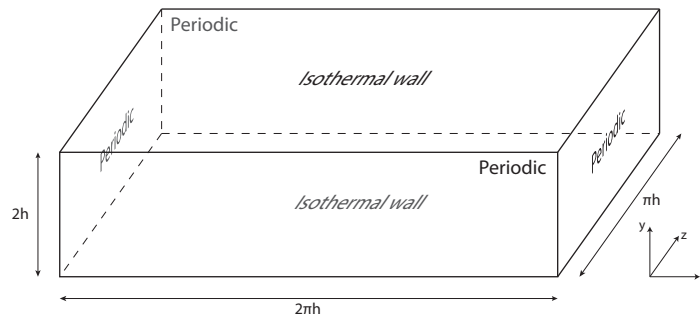


Figure 12: Sketch of the channel sizes and boundary conditions

The domain was discretized by a uniform Cartesian grid featuring $N_x \times N_y \times N_z$ grid points, that are listed in the following table:

Mach	Re_τ^{target}	Re_τ^{true}	Grid points	Δx^+	Δy^+	Δz^+
0.1	395	389.2	32x32x16	77.6	24.7	77.6
0.1	590	575.2	48x48x24	77.2	24.6	77.2
0.1	1000	943.1	80x60x40	78.5	33.3	78.5
0.1	2000	1821.0	128x66x64	98.2	60.6	98.2

Table 1: Selection of grid points and the resulting spacing in wall units at different friction Reynolds numbers

where the number of grid points in the wall-normal direction is chosen such as the second point (the top boundary in our WMLES implementation) fall within the log-layer region ($y^+ > 30$); the number of points in the other directions is chosen consequently to give an acceptable stretching factor. The numerical scheme used is the sixth-order fully split-convective energy-preserving scheme by Kennedy, Grüber and Pirozzoli (KGP6). To promote the turbulence transition, the initial conditions for the primitive variables have been imposed following the procedure proposed by Dan and John [9] (that consists in superimposing a vortex pair to the analytical solution of the Poiseuille flow).

The solution was advanced in time until a statistical convergence of the flow variables has been reached. The time step was evaluated employing the Courant- Friedrichs-Lewy condition and setting a CFL number equal to 0.5 [22].

7.1 Pressure-driven turbulent channel

To reproduce numerically a channel flow, the mean pressure gradient must be imposed (it's also possible to impose the mean wall shear stress, see equation (3.9)). This condition is imposed expressing the mean pressure gradient in term of non-dimensional reference quantities. Considering the definition of the bulk velocity as the volume integral of the u -momentum divided by the volume integral of the density:

$$u_b = \frac{\int_V \rho u dV}{\int_V \rho dV} \quad (7.1)$$

we can express the mean pressure gradient as a function of the deficit between a reference speed u_∞ and the bulk speed

$$\frac{dP}{dx} = u_\infty - u_b = \mathcal{F} \quad (7.2)$$

which defines suitable forcing terms for the Navier-Stokes system of equations

$$\mathbf{S}^T = \{0, \rho \mathcal{F}, 0, 0, \mathcal{F}\} \quad (7.3)$$

that can be added to the right-hand-side of the Navier Stokes equations to enforce that the bulk speed of the channel fits dynamically the reference speed u_∞ . This implementation allow the application of periodic boundary conditions along both stream and span-wise directions avoiding any synthetic turbulence injection at the inflow position. Finally, the reference speed u_∞ can be expressed as a function of the Mach number according to the

expression $u_\infty = \sqrt{\gamma}M_\infty$ while the Reynolds number associated with the bulk velocity can be defined as

$$Re_b = \frac{2u_b h}{\nu_\infty}. \quad (7.4)$$

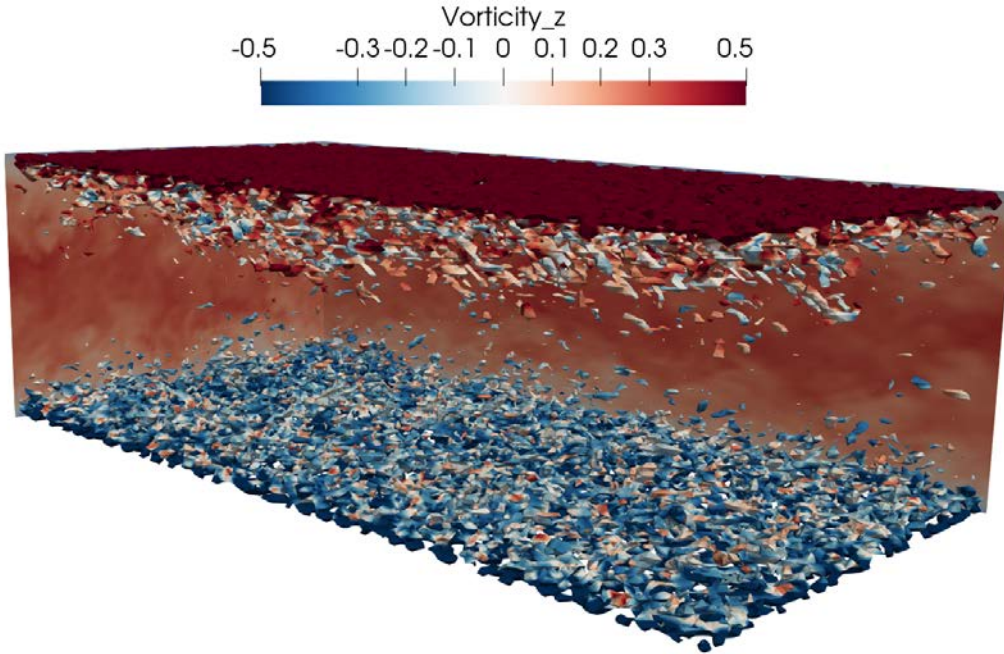


Figure 13: Visualization of the WMLES simulation of the turbulent channel at $Re_\tau = 2000$. Here the Q-criterion shows the 1.5 iso-contours of the second invariant of the velocity-gradient. The color map refers to the non-dimensional z-vorticity component

The following graphs show the scaled velocity u^+ and the Reynolds stresses $\langle u_i u_j \rangle$ against y^+ for the friction Reynolds numbers listed in Table 4.

7.2 $Re_\tau = 395$

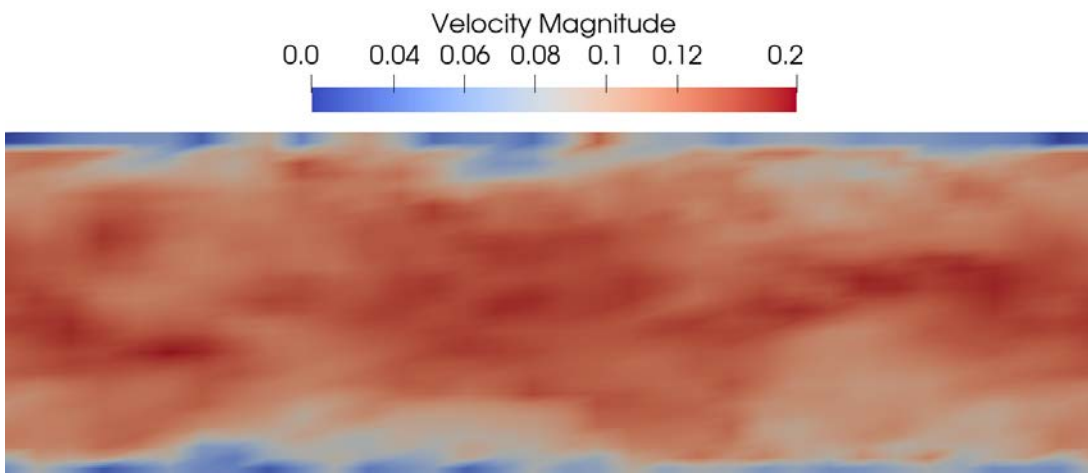


Figure 14: Example of velocity contour of a turbulent channel flow: $M = 0.1$, $Re = 395$

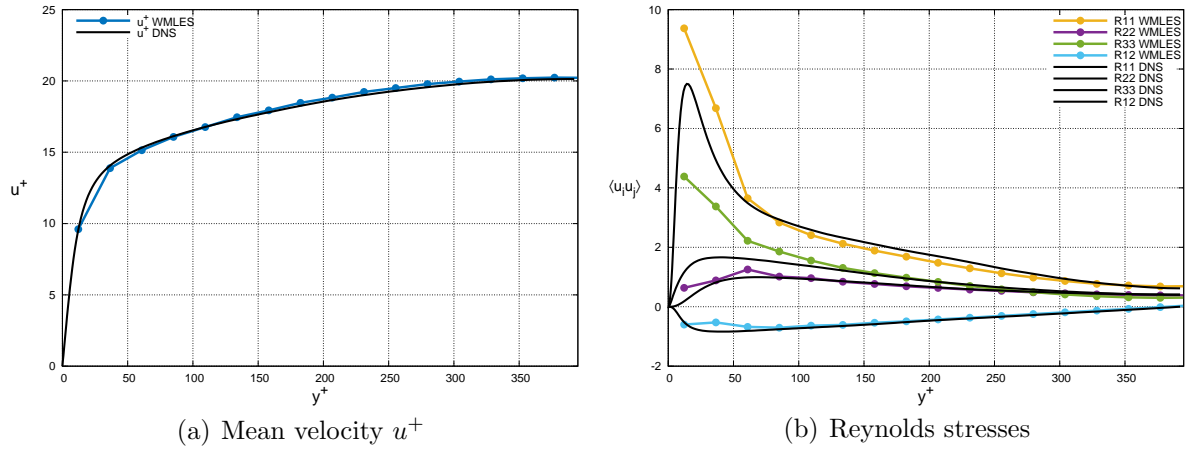


Figure 15: Mean velocity and Reynolds stresses against y^+ : DNS data of Moser et al. [17]: $Re_\tau = 395$

7.3 $Re_\tau = 590$

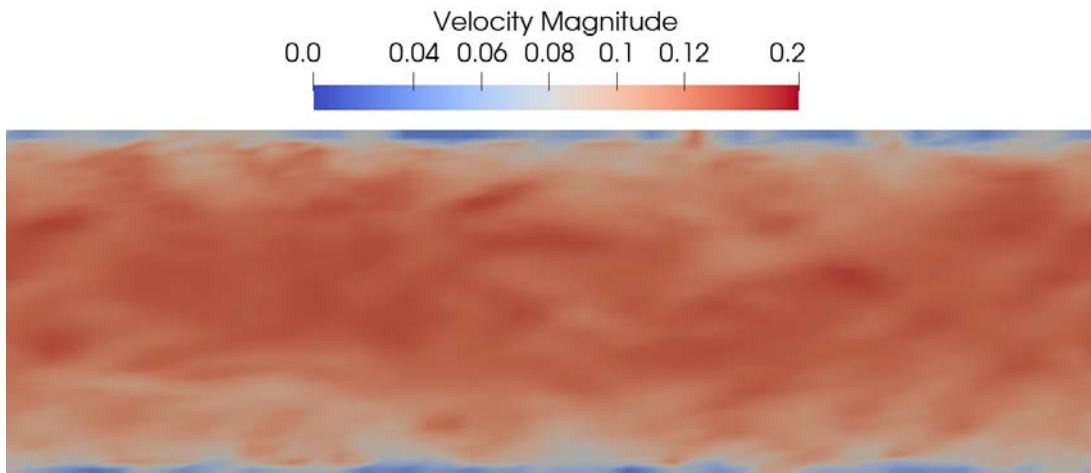


Figure 16: Example of velocity contour of a turbulent channel flow: $M = 0.1$, $Re = 590$

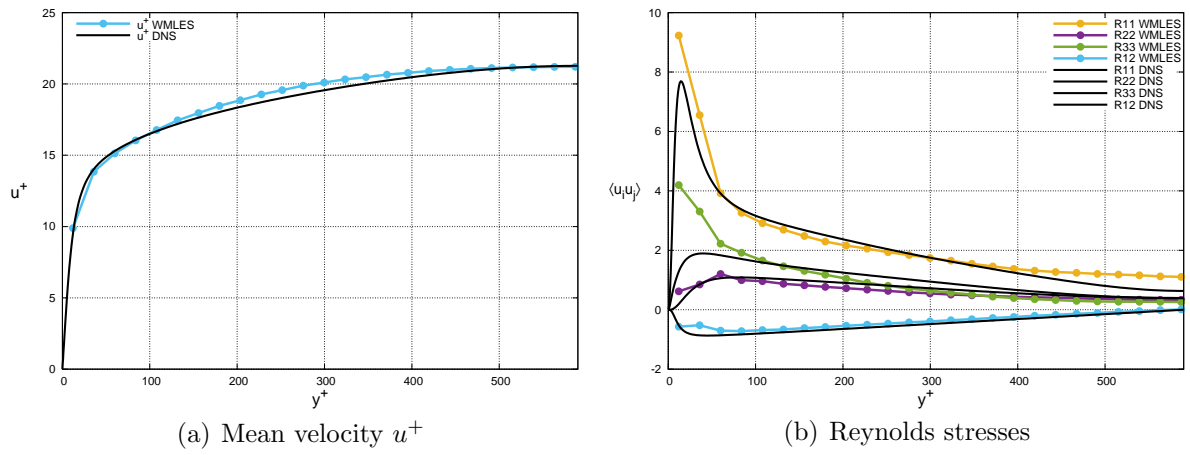


Figure 17: Mean velocity and Reynolds stresses against y^+ : DNS data of Vreman [23]: $Re_\tau = 590$

7.4 $Re_\tau = 1000$

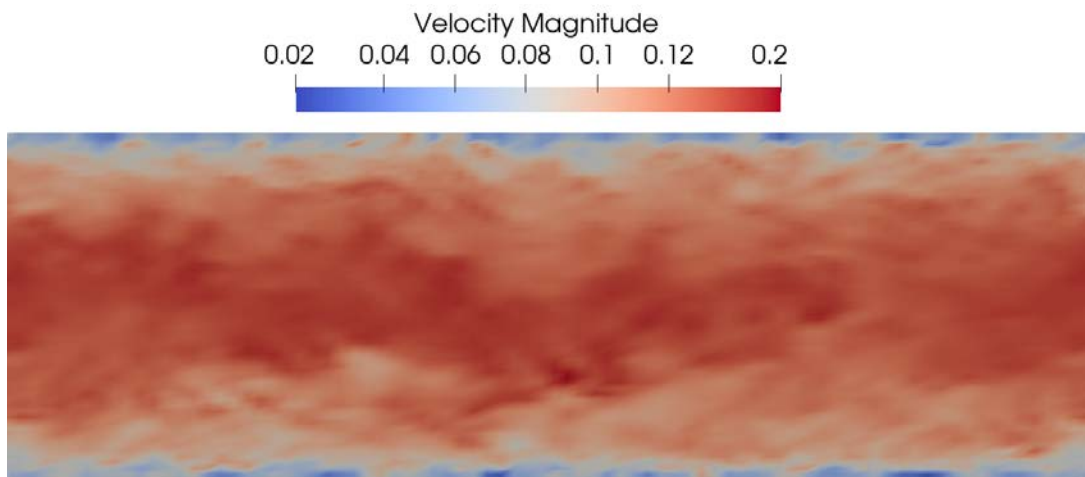


Figure 18: Example of velocity contour of a turbulent channel flow: $M = 0.1$, $Re = 1000$

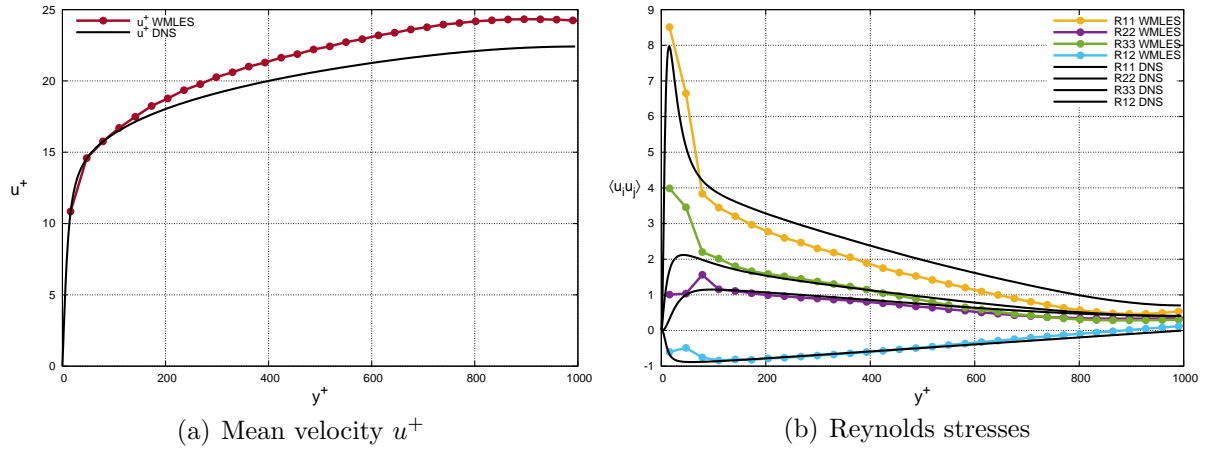


Figure 19: Mean velocity and Reynolds stresses against y^+ : DNS data of Bernardini et al. [14]: $Re_\tau = 1000$

7.5 $Re_\tau = 2000$

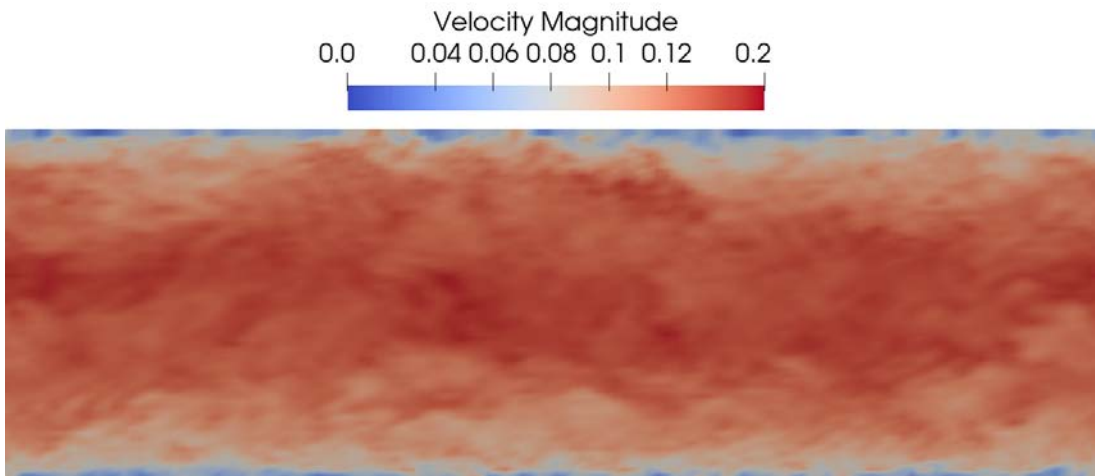


Figure 20: Example of velocity contour of a turbulent channel flow: $M = 0.1$, $Re = 2000$

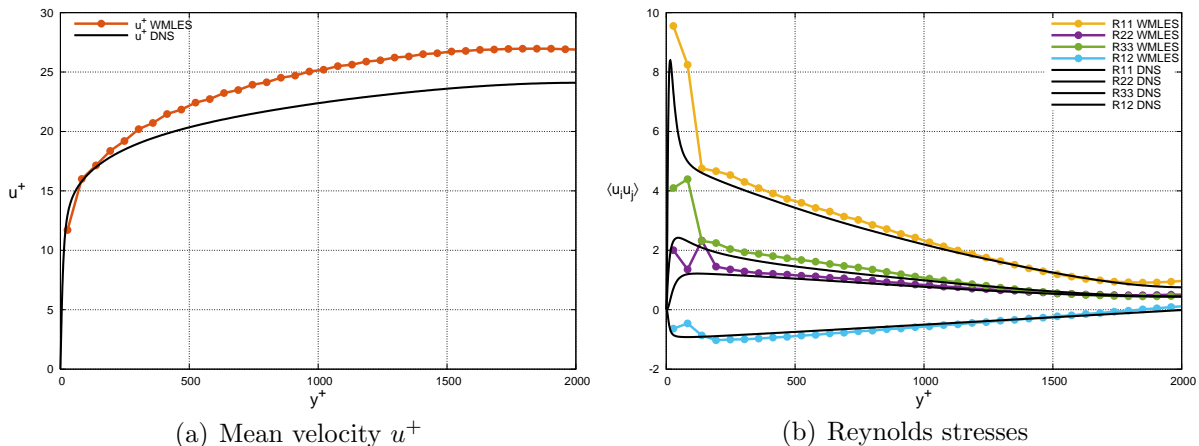


Figure 21: Mean velocity and Reynolds stresses against y^+ : DNS data of Bernardini et al. [14]: $Re_\tau = 2000$

7.6 Comments to the results

Overall the results are in good agreement with the DNS data, showing only small disagreements especially in the mean velocity profile, that is found to have a positive mismatch with the DNS data in the inner part of the channel that is more prominent as Re_τ increases. Looking at the Reynolds stresses, the fluctuations of resolved turbulence away from the wall are obtained in a reasonable agreement with the DNS data whereas the near-wall fluctuations in the unresolved-inner layer are not computed. This implies that the wall model works as expected, creating physically realistic fluctuations of the resolved turbulence without resolving the near-wall region.

The real advantage of WMLES approach can be seen comparing it to the number of points required using the DNS and WRLES approaches. For example looking at the data presented in Table 2 of Modesti [16] we can see that in a channel of sizes $6\pi h \times 2h \times 2\pi h$ at $Re = 999$ were used $2048 \times 384 \times 1024$ points, which is approximately 700 times more the number of total points used in our implementation (see Table 4). Furthermore this advantage in computational cost is observed also compared to a *wall resolved* LES, that requires a spacing in the wall normal direction of $y^+ < 1$ (like DNS) but accepts a more coarse grid in the other directions.

Mach	Re_τ	WMLES	WRLES	DNS
		$\Delta x^+, \Delta y^+, \Delta z^+$	$\Delta x^+, \Delta y^+, \Delta z^+$	$\Delta x^+, \Delta y^+, \Delta z^+$
0.1	395	$77.6 \times 24.7 \times 77.6$	$40 \times 1 \times 20$	$7.2 \times 1 \times 4.8$
0.1	590	$77.2 \times 24.6 \times 77.2$	$40 \times 1 \times 20$	$4.8 \times 1 \times 2.4$
0.1	1000	$78.5 \times 33.3 \times 78.5$	$40 \times 1 \times 20$	$9.2 \times 1 \times 6.1$
0.1	2000	$98.2 \times 60.6 \times 98.2$	$40 \times 1 \times 20$	$9.2 \times 1 \times 6.2$

Table 2: Comparison of the spacing in wall units needed to perform a WMLES, WRLES and DNS simulation at different friction Reynolds numbers. The DNS data are reported from Moser [17], Vreman [23] and Bernardini [14]

8 Simulation at Mach = 1.5

In this section are presented the results of the simulations computed with URANOS at $M = 1.5$ and two Reynolds numbers (500 and 1010). The channel sizes are $2\pi h \times 2h \times \pi h$ and the boundary conditions enforced to its faces are the same as the incompressible case. The domain was discretized by a uniform Cartesian grid featuring $N_x \times N_y \times N_z$ grid points, that are listed in the following table:

Mach	Re_τ^{target}	Re_τ^{true}	Grid points	Δx^+	Δy^+	Δz^+
1.5	500	496.4	40x40x20	78.5	25.0	78.5
1.5	1010	1013.4	80x80x40	79.3	25.3	79.3

Table 3: Selection of grid points and the resulting spacing in wall units for the selected friction Reynolds numbers

The following graphs show the scaled velocity u^+ , the Reynolds stresses $\langle u_i u_j \rangle$ and the temperature against y^+ for the friction Reynolds numbers listed in Table 3.

8.1 $Re = 500$

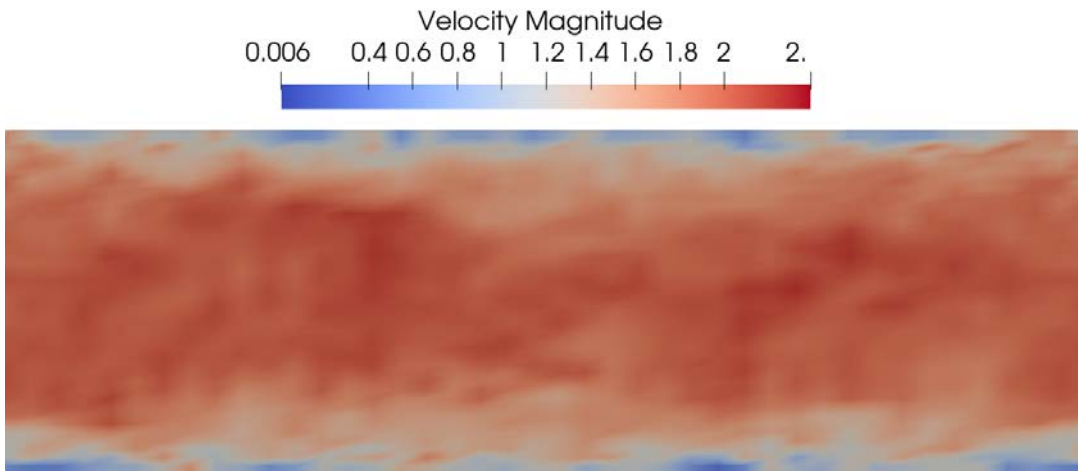


Figure 22: Example of velocity contour of a turbulent channel flow: $M = 1.5$, $Re = 500$

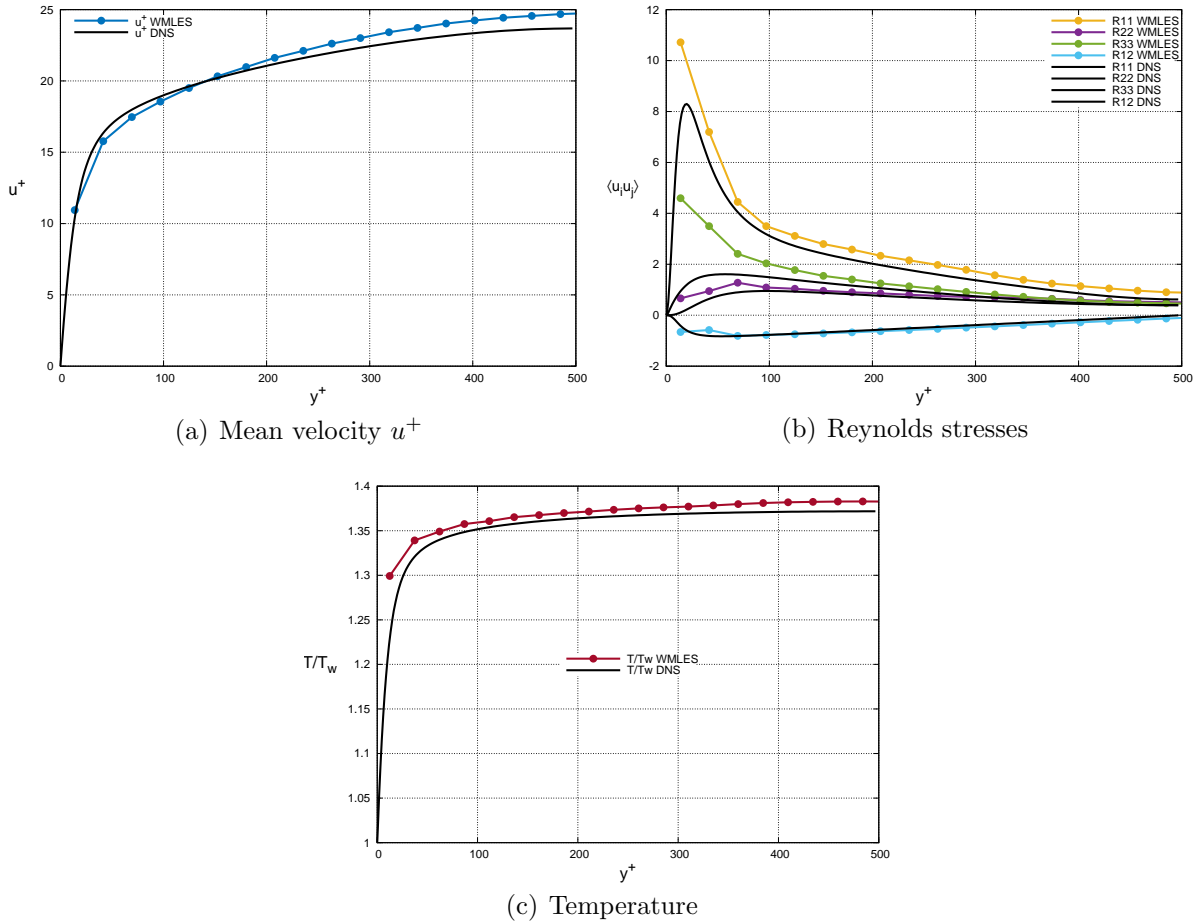


Figure 23: Mean velocity, Reynolds stresses and mean temperature profiles against y^+ : DNS data of Modesti et al. [15]: $Re_\tau = 500$

8.2 $Re = 1010$

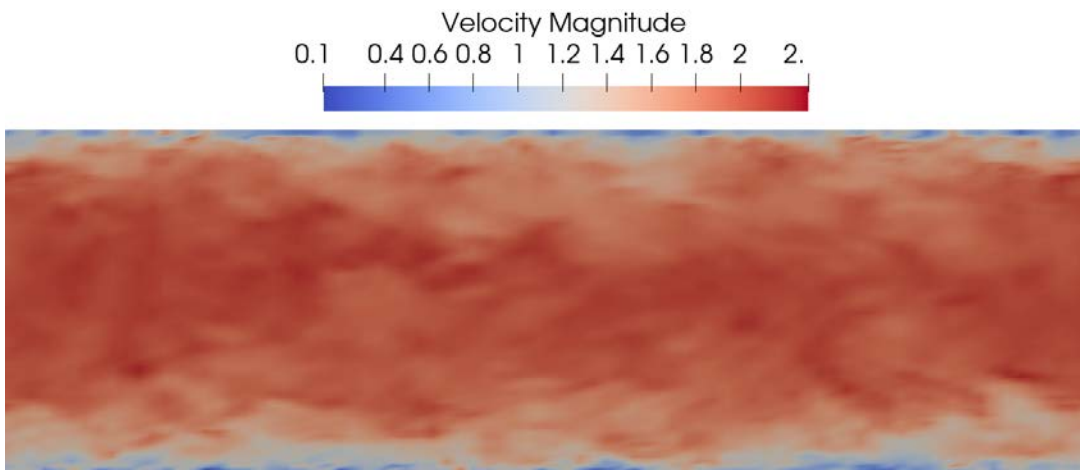


Figure 24: Example of velocity contour of a turbulent channel flow: $M = 1.5$, $Re = 1010$

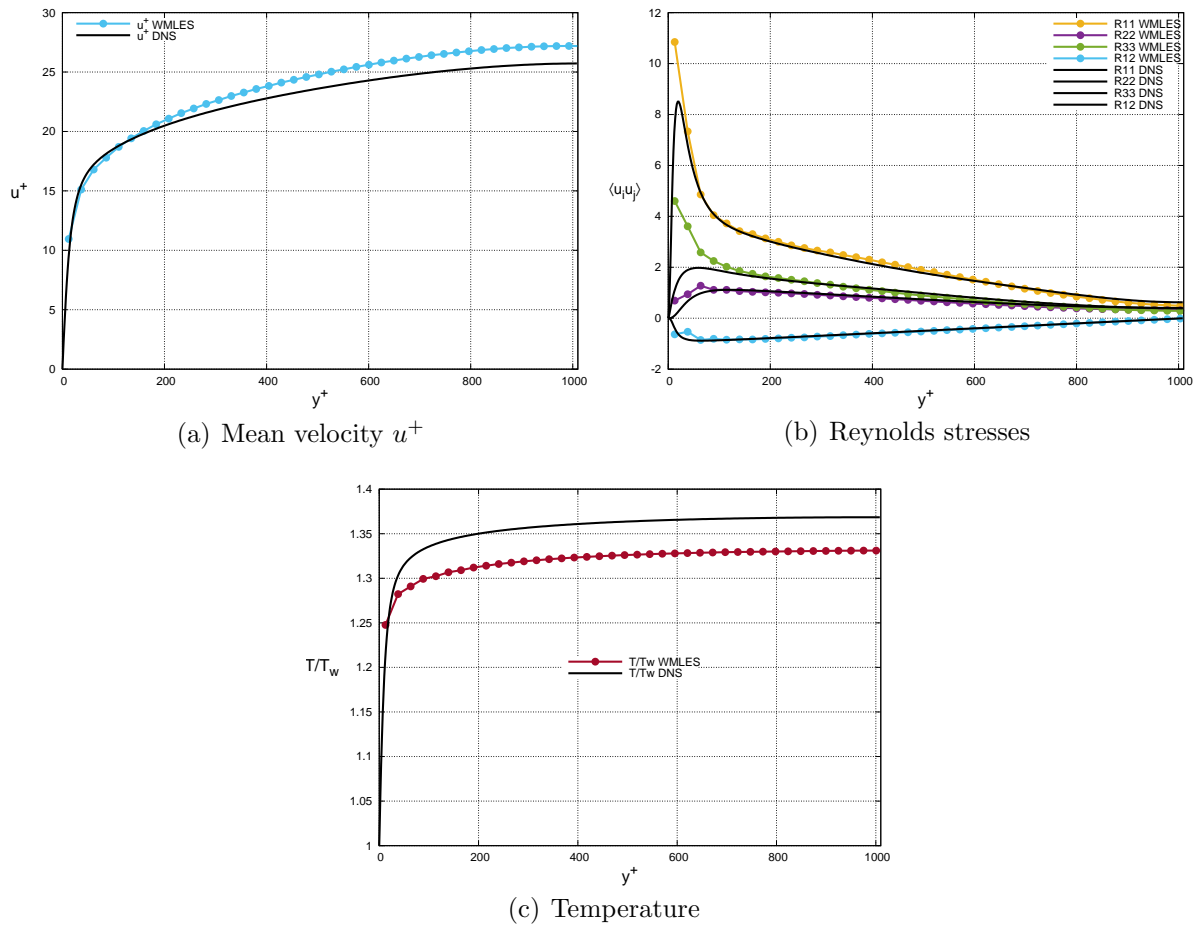


Figure 25: Mean velocity, Reynolds stresses and mean temperature profiles against y^+ : DNS data of Modesti et al. [15]: $Re_\tau = 1010$

8.3 Comments to the results

In both cases we can see that the mean velocity profile is well predicted at the first point near the wall by the wall stress model but there is a positive mismatch going through the center of the channel. The Reynolds stresses are very well predicted, considering, like the previous section, that the near wall region is not resolved so its expected a departure from DNS data. The temperature profile is in good agreement with the DNS data (it has a positive mismatch in the $Re = 500$ case and a negative one in the $Re = 1010$ case) but the model fails to predict accurately the temperature in the near wall region, thus needs to be further investigated. Like in the incompressible case it's worth pointing out the great advantage that the WMLES gives in terms of computational cost, which can be seen in the next table where WMLES grid size is compared to the WRLES and DNS one.

Mach	Re_τ	WMLES	WRLES	DNS
		$\Delta x^+, \Delta y^+, \Delta z^+$	$\Delta x^+, \Delta y^+, \Delta z^+$	$\Delta x^+, \Delta y^+, \Delta z^+$
1.5	500	$78.5 \times 25.0 \times 78.5$	$40 \times 1 \times 20$	$9.2 \times 1 \times 6.1$
1.5	1010	$79.3 \times 25.3 \times 79.3$	$40 \times 1 \times 20$	$9.3 \times 1 \times 6.2$

Table 4: Comparison of the spacing in wall units needed to perform a WMLES, WRLES and DNS simulation at different friction Reynolds numbers. The DNS data are reported from Modesti et al. [15]

9 Conclusions

The goal of this thesis was to determine the applicability and practicality of an ODE-based modelling technique for LES of channel flows. We tested our implementation in both incompressible and compressible case finding a general good agreement with DNS data, with the expected log-layer mismatch of velocity and temperature profile that is still not well understood (see section 3.2 of Larsson et al. [12]). The compressible case has proven to be the most difficult to model due to the difficulty to impose the right boundary condition for the wall heat flux (that has the difficult task to provide an averaged thermal equilibrium even if the temperature gradient is modelled) and its sensitivity to the grid. We think that some challenges that had to be faced during the implementation of boundary conditions were due to the fact that the code has been developed with a finite differences method, but in turn this is a unique feature that is rarely found in other implementations especially with the intent to keep the numerical scheme as general as possible (i.e. not made ad hoc for the wall-modelling approach). However we verified in every simulation the real advantage of this approach: the computational cost. While the accuracy of LES is undoubtedly better than that of equivalent RANS simulations in most cases, the cost is at least an order of magnitude higher. In this context, WMLES reduction of computational cost makes it comparable to RANS approach but keeping the multiscale and non stationary features of LES. In an industry where calculation turn around times have to be measured in at most a few days (while LES typically requires some weeks), WMLES can be a real breakthrough in the prediction of every type of flow whose unsteady, multiscale and fluctuating nature needs to be simulated in a reasonable amount of time. These growing markets ensure a future for this methodology, while its implementation in the mainstream of commercial CFD will be possible by methodological advances and increased computational resources.

A Appendix - Navier-Stokes Equations

A.1 Divergence Theorem

The integral over a closed surface δV of the product of a vector field \mathbf{F} with the normal \mathbf{n} to the surface is equal to the integral over the volume enclosed by the surface V of the divergence of the field:

$$\int_{\delta V} \mathbf{F} \cdot \hat{\mathbf{n}} dA = \int_V \vec{\nabla} \cdot \mathbf{F} dV \quad (\text{A.1})$$

A.2 Reynolds transport theorem

Consider a volume V delimited by a closed surface δV , both time dependent. The Reynolds transport theorem states that given a function of space and time $F(\vec{x}, t)$, the total derivative of the integral over a time varying volume of the function is equal to the integral over the same volume of the partial derivative of the function in time added to the surface integral of the function multiplied by the dot product between the velocity of the surface \mathbf{b} and its normal \mathbf{n} .

$$\frac{d}{dt} \int_{V(t)} F(\vec{x}, t) dV = \int_{V(t)} \frac{\partial F(\vec{x}, t)}{\partial t} + \int_{\delta V(t)} F(\vec{x}, t) \vec{b} \cdot \hat{\mathbf{n}} dA \quad (\text{A.2})$$

The first term represents the time variation of the function in the volume, while the second accounts for the time variation of the contour of the volume itself.

A.3 Conservation of mass

The law of conservation of mass states that the time variation of mass in a certain control volume has to be zero [1], so we can write:

$$\frac{dM}{dt} = 0 \quad , \quad \text{where} \quad M = \int_V \rho dV \quad (\text{A.3})$$

using the Reynolds transport theorem A.2 for the function $\rho(\vec{x}, t)$ we get:

$$\frac{d}{dt} \int_V \rho dV = \int_V \frac{\partial \rho}{\partial t} dV + \int_{\delta V} \rho \vec{u} \cdot \hat{\mathbf{n}} dA = 0 \quad (\text{A.4})$$

then applying the divergence theorem A.1 for the second term we get:

$$\int_V \frac{\partial \rho}{\partial t} dV + \int_V \vec{\nabla} \cdot (\rho \vec{u}) dV = \int_V \left[\frac{\partial \rho}{\partial t} + \vec{\nabla} \cdot (\rho \vec{u}) \right] dV = 0 \quad (\text{A.5})$$

and differentiating we obtain the law of conservation of mass:

$$\frac{\partial \rho}{\partial t} + \vec{\nabla} \cdot (\rho \vec{u}) = 0 \quad (\text{A.6})$$

that using the index notation becomes:

$$\frac{\partial \rho}{\partial t} + \frac{\partial \rho u_j}{\partial x_j} = 0 \quad (\text{A.7})$$

A.4 Conservation of Momentum

The law of conservation of momentum $\vec{Q} = m\vec{u}$ states that its variation in time is equal to the sum of external forces:

$$\frac{d\vec{Q}}{dt} = \sum \vec{F}_e \quad (\text{A.8})$$

where the momentum is defined as

$$\vec{Q} = \int_V \rho \vec{u} dV \quad (\text{A.9})$$

we can use the Reynolds transport theorem [A.2](#) and the divergence theorem [A.1](#) to write the first part of the equation [A.8](#) as:

$$\int_V \left[\frac{\partial \rho \vec{u}}{\partial t} + \vec{\nabla} \cdot \rho \vec{u} \vec{u} \right] dV = \sum \vec{F}_e \quad (\text{A.10})$$

The external forces can be divided in volume forces and surface forces:

$$\sum \vec{F}_e = \begin{cases} d\vec{F}_{e,V} = \rho \vec{f} dV \\ d\vec{F}_{e,A} = \vec{t}_n dA = \vec{T} \cdot \hat{n} dA \end{cases}$$

For newtonian fluids, \vec{T} has the following expression:

$$\vec{T} = -p\vec{I} + 2\mu\vec{E} - \frac{2}{3}\mu (\vec{\nabla} \cdot \vec{u}) \vec{I} = -p\vec{I} + \vec{\Sigma} \quad (\text{A.11})$$

where \vec{I} is the identity matrix and $\vec{E} = \frac{1}{2} (\vec{\nabla} \vec{u} + \vec{\nabla} \vec{u}^T)$. substituting all the forces in the [A.10](#) and differentiating we get the law of conservation of momentum:

$$\frac{\partial \rho \vec{u}}{\partial t} + \vec{\nabla} \cdot (\rho \vec{u} \vec{u}) = \rho \vec{f} - \vec{\nabla} \vec{p} + \vec{\nabla} \cdot \vec{\Sigma} \quad (\text{A.12})$$

that written in the index notation becomes:

$$\frac{\partial \rho u_i}{\partial t} + \frac{\partial (\rho u_i u_j)}{\partial x_j} = \rho f_i + \frac{\partial}{\partial x_j} (-p\delta_{ij} + \Sigma_{ij}) \quad (\text{A.13})$$

A.5 Conservation of energy

The law of conservation of energy states that the time variation of the total energy of the system is equal to the amount of heat transmitted to the system plus the total work done to the system.

$$\frac{dE_T}{dt} = \dot{Q} + \dot{W} \quad (\text{A.14})$$

The total energy can be expressed as the sum of the internal energy and the kinetic energy:

$$E_T = \int_V \rho \left(e + \frac{u^2}{2} \right) dV \quad (\text{A.15})$$

using the Reynolds theorem, its variation in time can be written as:

$$\frac{d}{dt} \int_V \rho \left(e + \frac{u^2}{2} \right) dV = \int_V \left\{ \frac{\partial}{\partial t} \left[\rho \left(e + \frac{u^2}{2} \right) \right] + \vec{\nabla} \cdot \left[\rho \left(e + \frac{u^2}{2} \right) \vec{u} \right] \right\} dV \quad (\text{A.16})$$

the heat term $\dot{Q} = \int_S d\dot{q}$ can be divided in volume and surface type:

$$d\dot{q} = \begin{cases} d\dot{q}_V = \rho Q dV \\ d\dot{q}_S = -\vec{q} \cdot \hat{n} dS \end{cases}$$

the same can be done for the work:

$$d\dot{W} = \begin{cases} d\dot{W}_V = \rho \vec{f} \cdot \vec{u} \\ d\dot{W}_S = \vec{u} \cdot \vec{t}_n dS = \vec{u} \cdot \vec{T} \cdot \hat{n} dS \end{cases}$$

substituting the heat and work term in the A.15 (remembering the expression A.11) and differentiating we get the law of conservation of energy:

$$\frac{\partial}{\partial t} \left[\rho \left(e + \frac{u^2}{2} \right) \right] + \vec{\nabla} \cdot \left[\rho \left(e + \frac{u^2}{2} \right) \vec{u} \right] = \rho Q - \vec{\nabla} \cdot \vec{q} + \rho \vec{u} \cdot \vec{f} - \vec{\nabla} \cdot (\vec{u}p) + \vec{\nabla} \cdot (\vec{u}\vec{\Sigma}) \quad (\text{A.17})$$

Noting that $\vec{\nabla} \cdot (\vec{u}p)$ can be expressed as:

$$\vec{\nabla} \cdot (\vec{u}p) = \rho \frac{D}{Dt} \left(\frac{P}{\rho} \right) - \frac{\partial p}{\partial t} \quad (\text{A.18})$$

where D/Dt is the total derivative, we can bring the pressure term to the left:

$$\frac{D}{Dt} \left[\rho \left(e + \frac{p}{\rho} + \frac{u^2}{2} \right) \right] = \rho Q - \vec{\nabla} \cdot \vec{q} + \rho \vec{u} \cdot \vec{f} + \vec{\nabla} \cdot (\vec{u}\vec{\Sigma}) + \frac{\partial p}{\partial t} \quad (\text{A.19})$$

we can define entalpy as $h = e + \frac{p}{\rho}$ and write the final expression of the energy law:

$$\frac{D}{Dt} \left[\rho \left(h + \frac{u^2}{2} \right) \right] = \rho Q - \vec{\nabla} \cdot \vec{q} + \rho \vec{u} \cdot \vec{f} + \vec{\nabla} \cdot (\vec{u}\vec{\Sigma}) + \frac{\partial p}{\partial t} \quad (\text{A.20})$$

using the index notation it becomes:

$$\frac{\partial}{\partial t} \left[\rho \left(h + \frac{u^2}{2} \right) \right] + \frac{\partial}{\partial x_j} \left[\rho \left(h + \frac{u^2}{2} \right) u_j \right] = \rho Q - \frac{\partial \vec{q}}{\partial x_j} + \rho u_i f_i + \frac{\partial (u_i \Sigma_{ij})}{\partial x_j} + \frac{\partial p}{\partial t} \quad (\text{A.21})$$

We can finally write the Navier-Stokes equation in index notation:

$$\begin{cases} \frac{\partial \rho}{\partial t} + \frac{\partial \rho u_j}{\partial x_j} = 0 \\ \frac{\partial \rho u_i}{\partial t} + \frac{\partial (\rho u_i u_j)}{\partial x_j} = \rho f_i + \frac{\partial}{\partial x_j} (-p \delta_{ij} + \Sigma_{ij}) \\ \frac{\partial}{\partial t} \left[\rho \left(h + \frac{u^2}{2} \right) \right] + \frac{\partial}{\partial x_j} \left[\rho \left(h + \frac{u^2}{2} \right) u_j \right] = \rho Q - \frac{\partial \vec{q}}{\partial x_j} + \rho u_i f_i + \frac{\partial (u_i \Sigma_{ij})}{\partial x_j} + \frac{\partial p}{\partial t} \end{cases}$$

This system consists in 5 equation in 7 unknowns, so to become solvable with must write two other equations. For an ideal gas these equations are:

$$\begin{cases} p = \rho RT \\ e = c_v T \end{cases}$$

References

- [1] John David Anderson Jr. *Fundamentals of aerodynamics*. Tata McGraw-Hill Education, 2010.
- [2] Sanjeeb T Bose and George Ilhwan Park. “Wall-modeled large-eddy simulation for complex turbulent flows”. In: *Annual review of fluid mechanics* 50 (2018), pp. 535–561.
- [3] Dean R Chapman. “Computational aerodynamics development and outlook”. In: *AIAA journal* 17.12 (1979), pp. 1293–1313.
- [4] Haecheon Choi and Parviz Moin. “Grid-point requirements for large eddy simulation: Chapman’s estimates revisited”. In: *Physics of fluids* 24.1 (2012), p. 011702.
- [5] Francesco De Vanna, Francesco Picano, and Ernesto Benini. “A sharp-interface immersed boundary method for moving objects in compressible viscous flows”. In: *Computers & Fluids* (2020), p. 104415.
- [6] Francesco De Vanna, Francesco Picano, and Ernesto Benini. “An Immersed Boundary Method for Moving Objects in Compressible Flows”. In: *ERCOTAC Workshop Direct and Large Eddy Simulation*. Springer. 2019, pp. 291–296.
- [7] Eugene De Villiers. “The potential of large eddy simulation for the modeling of wall bounded flows”. In: *Imperial College of Science, Technology and Medicine* (2006).
- [8] Eric Garnier, Nikolaus Adams, and Pierre Sagaut. *Large eddy simulation for compressible flows*. Springer Science & Business Media, 2009.
- [9] Dan S Henningson and John Kim. “On turbulent spots in plane Poiseuille flow”. In: *Journal of fluid mechanics* 228 (1991), pp. 183–205.
- [10] J.O. Hinze. *Turbulence*. 1972.
- [11] Andrey Nikolaevich Kolmogorov. “The local structure of turbulence in incompressible viscous fluid for very large Reynolds numbers”. In: *Cr Acad. Sci. URSS* 30 (1941), pp. 301–305.
- [12] Johan Larsson et al. “Large eddy simulation with modeled wall-stress: recent progress and future directions”. In: *Mechanical Engineering Reviews* 3.1 (2016), pp. 15–00418.
- [13] Marcel Lesieur. *Turbulence in fluids*. Vol. 40. Springer Science & Business Media, 2012.
- [14] P. Orlandi M. Bernardini S. Pirozzoli. *Turbulent channel flow - DNS database up to $Re_\tau = 4000$* . Last update: 2014-10-08. URL: <http://newton.dma.uniroma1.it/channel/>.
- [15] D. Modesti and S. Pirozzoli. *Supersonic turbulent channel flow - DNS database up to $Re_\tau = 1000$* . Last update: 2020-08-14. URL: <http://newton.dima.uniroma1.it/supchan/stat/>.
- [16] Davide Modesti and Sergio Pirozzoli. “Reynolds and Mach number effects in compressible turbulent channel flow”. In: *International Journal of Heat and Fluid Flow* 59 (2016), pp. 33–49.

- [17] Kim Mansour Moser. *DNS Data for Turbulent Channel Flow*. Last update: Feb. 1, 2007. URL: http://turbulence.oden.utexas.edu/MKM_1999.html.
- [18] Franck Nicoud and Frédéric Ducros. “Subgrid-scale stress modelling based on the square of the velocity gradient tensor”. In: *Flow, turbulence and Combustion* 62.3 (1999), pp. 183–200.
- [19] Stephen B Pope. *Turbulent flows*. 2001.
- [20] Ludwig Prandtl. “7. Bericht über Untersuchungen zur ausgebildeten Turbulenz”. In: *ZAMM-Journal of Applied Mathematics and Mechanics/Zeitschrift für Angewandte Mathematik und Mechanik* 5.2 (1925), pp. 136–139.
- [21] Lewis Fry Richardson. *Weather prediction by numerical process*. Cambridge university press, 2007.
- [22] Francesco De Vanna. “A high-resolution fully compressible Navier-Stokes solver for analysis of moving objects at high Mach numbers”. In: *PhD thesis* (2019).
- [23] Bert Vreman. *Databases of Direct Numerical Simulations of turbulent channel flow*. Last update: 4 November 2015. URL: <http://www.vremanresearch.nl/channel.html>.
- [24] Xiang IA Yang and Yu Lv. “A semi-locally scaled eddy viscosity formulation for LES wall models and flows at high speeds”. In: *Theoretical and Computational Fluid Dynamics* 32.5 (2018), pp. 617–627.
- [25] XIA Yang et al. “Aerodynamic heating in wall-modeled large-eddy simulation of high-speed flows”. In: *AIAA journal* 56.2 (2018), pp. 731–742.

ACKNOWLEDGEMENTS

Considering the accomplishment of this thesis I would like to thank my advisor and co-advisor for the opportunity they gave me and the constant support during my work.

I would also like to thank my girlfriend, *Linda*, my university colleagues and friends (a special thanks goes to *Alberto S.*, *Giovanni M.*, *Leonardo D.*, *Simone C.* and *Lorenzo G.*) and my family.

Lastly, I want to thank my brother *Massimiliano* for sustaining me in the hard moments even if he's only present in my heart.

M.C.